ELSEVIER

Journal of Neuroimmunology 182 (2007) 212–218

Journal of
Neuroimmunology

www.elsevier.com/locate/jneuroim

Anti-ganglioside complex antibodies associated with severe disability in GBS☆

K. Kaida [a], D. Morita [b], M. Kanzaki [a], K. Kamakura [a], K. Motoyoshi [a], M. Hirakawa [b], S. Kusunoki [b,*]

[a] *Third Department of Internal Medicine, National Defense Medical College, 3-2 Namiki, Saitama-ken, 359-8513, Japan*
[b] *Department of Neurology, Kinki University School of Medicine, 377-2 Ohno-Higashi, Osaka-Sayama, Osaka, 589-8511, Japan*

Received 18 April 2006; received in revised form 8 September 2006; accepted 27 September 2006

Abstract

Ganglioside complexes (GSCs) are known as target antigens in Guillain–Barré syndrome (GBS). To elucidate the clinical importance of the anti-GSC antibodies in GBS, we investigated serum antibodies to GSCs containing two of the gangliosides, GM1, GD1a, GD1b and GT1b, and analyzed clinical features of anti-GSC-positive GBS patients. Thirty-nine (17%) of 234 GBS patients had IgG anti-GSC antibodies. Anti-GSC-positive GBS had antecedent gastrointestinal infection and lower cranial nerve deficits more frequently than control GBS. The presence of antibody specificity to GD1a/GD1b and/or GD1b/GT1b was significantly associated with severe disability and a requirement for mechanical ventilation.

Keywords: Guillain–Barré syndrome; Ganglioside complex; Antibody; Disability

1. Introduction

Gangliosides concentrate on the surfaces of neurons, with their oligosaccharide portions exposed on the cell surface, and are believed to form clusters extensively in the cell membrane (Hakomori, 2002). Recent studies of plasma membrane molecules have shown that gangliosides appear to be organized in clusters, and to form membrane microdomains together with cholesterol and glycosylphosphatidylinositol (GPI)-anchored proteins (Simons and Toomre, 2000). These microdomains are called lipid rafts or detergent-resistant membranes.

Gangliosides in peripheral nerves are often targeted by serum antibodies in patients with Guillain–Barré syndrome (GBS), acute immune-mediated polyradiculoneuropathy, and interaction between anti-ganglioside antibodies and peripheral nerve gangliosides is believed to cause GBS and its variants (Chiba et al., 1993; Willison and Yuki, 2002; Kaida et al., 2003). We recently demonstrated the presence of antibodies to ganglioside complexes (GSCs) in serum of some GBS patients and suggested that anti-GSC antibodies might function in the development of GBS (Kaida et al., 2004). It has hitherto been inferred that ligands of adhesion molecules such as selectins comprise diverse and complex glycoconjugates, called clustered saccharide patches, in which oligosaccharides are packed closely together to form rigid rodlike structures with multivalency and strict binding-specificity (Norgard et al., 1993; Varki, 1994). The discovery of anti-GSC antibodies in GBS serum suggests that clustered glycoepitopes of GSCs or clustered saccharide patches actually exist on the plasma membrane and are involved in immune-mediated events.

In our previous study (Kaida et al., 2004), eight of 100 GBS patients had IgG antibodies to GD1a–GD1b complexes (GD1a/GD1b) and were predisposed to lower cranial nerve palsy and severe disability. However, statistical significance

☆ Disclosure: The authors have reported no conflicts of interest.

* Corresponding author. Tel.: +81 72 366 0221x3553; fax: +81 72 368 4846.
E-mail address: kusunoki-tky@umin.ac.jp (S. Kusunoki).

0165-5728/$ - see front matter © 2006 Elsevier B.V. All rights reserved.
doi:10.1016/j.jneuroim.2006.09.013

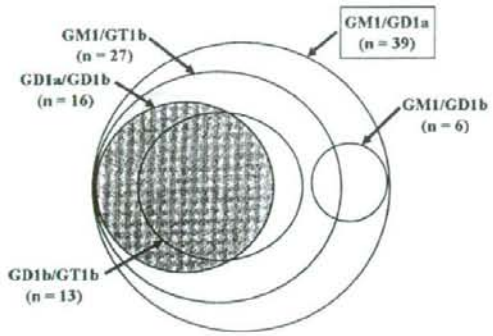

Fig. 1. The Venn diagram shows distribution of anti-GSC(+) group patients based on data in Table 1. All of the anti-GSC(+) group patients had IgG anti-GM1/GD1a antibodies. Anti-GD1a/GD1b-positive patients had also IgG anti-GM1/GD1a and GM1/GT1b antibodies. Ten anti-GSC(+) group patients had IgG anti-GD1a/GD1b and anti-GD1b/GT1b antibodies.

of the association between that antibody and those clinical features has not been demonstrated. In the present study, to clarify the clinical significance of anti-GSC antibodies in GBS, we retrospectively analyzed the clinical features of anti-GSC antibody-positive patients with GBS in a larger population, with a focus on the fine specificity of anti-GSC antibodies and its clinical relevance.

2. Materials and methods

2.1. Patient serum and enzyme-linked immunosorbent assay for anti-ganglioside complex antibodies

Acute phase serum was collected from patients with clinically defined GBS between September 2001 and December 2002 at various general and teaching hospitals throughout Japan. All met the diagnostic criteria of Asbury and Cornblath (Asbury and Cornblath, 1990).

ELISA was done for serum antibodies to gangliosides GM1, GM2, GM3, GD1a, GalNAc–GD1a, GD1b, GD3, GT1b, and GQ1b, as described elsewhere (Kaida et al., 2000). The ELISA for anti-GSC antibodies were performed as described in our previous report (Kaida et al., 2004). GSCs used in the ELISA contained two (0.1 μg each) of four ganglioside antigens, GM1, GD1a, GD1b, and GT1b which

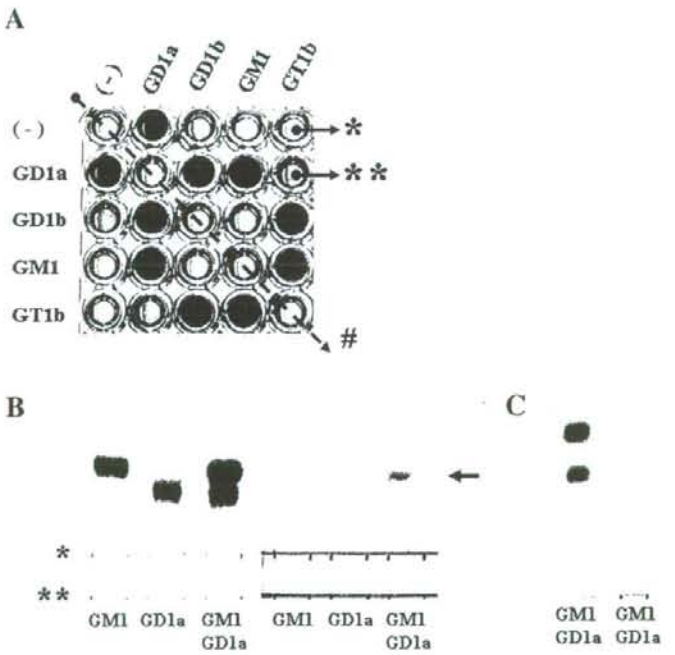

Fig. 2. Representative ELISA results and thin-layer chromatography (TLC) studies for antibodies to GSCs using sera from Anti-GSC(+) group patients. (A) Serum from patient no.16 in the Anti-GSC(+) group was used. A weak reaction is observed in a well containing only GD1a, while strong reactions can be seen in wells containing GD1a/GD1b, GM1/GD1a, GD1b/GT1b, and GM1/GT1b (w/w = 0.1/0.1). * = GT1b only (0.2 μg), ** = a mixture of GD1a (0.1 μg) and GT1b (0.1 μg). # Five control wells on each plate are indicated by oblique dotted arrows. (B) Serum from patient no.18 was used. TLC bands were visualized with orcinol reagent in the left panels. Immunostaining using anti-GSC antibody-positive sera (diluted 1:100 with 1% BSA in PBS) is shown in the right panels. Immunostaining is shown in the overlapping portions of GM1 and GD1a (arrow). GD1a was applied on the upper line (*) and GM1 on the lower line (**). (C) The immunostaining in the overlapping portions of GM1 and GD1a have disappeared in a solvent system that separated the positions of GM1 and GD1a to a great extent (serum from patient no.18). The developing solvent comprised chloroform, methanol, and 0.2%CaCl2.2H2O as follows; 55/40/10 (v/v, Fig. 2B), 50/45/10 (Fig. 2C).

Table 1
Frequency of antibodies to single gangliosides in anti-GSC(+) and control groups

	Antiganglioside antibody	Antibody specificity in anti-GSC(+) group*					Control
		GM1/GD1a (Anti-GSC(+))	GM1/GD1a GM1/GT1b	GM1/GD1a GM1/GT1b GD1a/GD1b	GM1/GD1a GM1/GT1b GD1b/GT1b	GM1/GD1a GM1/GT1b GD1a/GD1b GD1b/GT1b	
		(n=38)	(n=27)	(n=16)	(n=13)	(n=10)	(n=170)
IgG class	anti-GM1	6 (16%)	3 (11%)	3 (19%)	2 (15%)	1 (10%)	27 (16%)
	anti-GD1a	4 (11%)	4 (15%)	4 (25%)[#1]	4 (31%)[#2]	4 (40%)[#3]	10 (6.1%)
	anti-GD1b	28 (74%)[#4]	20 (74%)[#4]	8 (50%)[#3]	8 (62%)[#5]	5 (50%)[#1]	9 (5.5%)
	anti-GT1b	3 (7.9%)	3 (11%)[#6]	3 (19%)[#7]	3 (23%)[#8]	3 (30%)[#9]	3 (1.8%)
	anti-GQ1b	6 (16%)	5 (19%)	1 (6.3%)	1 (7.7%)	1 (10%)	15 (9.1%)
	anti-GalNAc-GD1a	7 (18%)	4 (15%)	1 (6.3%)	0	0	26 (16%)**
IgM class	anti-GM1	2 (5.3%)	2 (7.4%)	2 (13%)	2 (15%)	2 (20%)	21 (13%)
	anti-GalNAc–GD1a	1 (2.6%)	1 (3.7%)	0	0	0	15 (9.4%)**

* The Anti-GSC(+) group was divided into four subgroups based on antibody specficity of anti-GSC antibodies. In the GSC(+) group, IgG antibodies to GM2, GM3, and GD3 and IgM to GD1a, GD1b, GT1b, GQ1b, GM2, GM3, and GD3 were negative. # indicates that there are significant differences between an antibody-positive group and remainder. Remainders include control group patients and remaining anti-GSCantibody-positive patients. [#1], p=0.02; [#2], p=0.009; [#3], p=0.003; [#4], p<0.0001; [#5], p=0.0004; [#6], p=0.03; [#7], p=0.007; [#8], p=0.004; [#9], p=0.002 The chi-square test was used to test differences in proportions when the number in a cell was more than 6. If not, Fisher's exact test was used. **n=166 patients.

were major gangliosides in human nervous system (Yu and Iqbal, 1979). Gangliosides were mixed for 30 min before application to the ELISA. If a serum has both anti-GD1a and anti-GD1b antibody activities, the serum was judged to be anti-GD1a/GD1b antibody-positive when an OD value of anti-GD1a/GD1b antibody was more than the sum of those of anti-GD1a and anti-GD1b antibodies. As for estimation of antibodies to GM1/GD1a, GM1/GD1b, GM1/GT1b, GD1a/GT1b, and GD1b/GT1b, the same criteria were applied. ELISAs were performed in duplicate and mean ODs were calculated.

2.2. ELISA for anti-Campylobacter jejuni antibodies in serum from anti-ganglioside complex antibody-positive patients

IgG and IgM antibodies to *C. jejuni* were investigated in acute phase serum samples from anti-GSC antibody-positive patients with antecedent gastrointestinal infection using an ELISA kit for C. jejuni (Serion ELISA classic, Campylobacter jejuni IgG/IgM; Institut Virion/Serion, Würzburg, Germany). Serum from patients already diagnosed as having had *C. jejuni* enteritis from stool or serum specimens at other hospitals was excluded from the investigation. In cases where patients had positive or borderline ELISA results for IgM or IgG antibodies to *C. jejuni* and had suffered from diarrhea without respiratory symptoms, they were considered to have had antecedent gastrointestinal infection associated with *C. jejuni*.

2.3. Study population and analyses of clinical and electrophysiological features

Patients with IgG antibodies to at least one combination of two of the four gangliosides, GM1, GD1a, GD1b, and GT1b were defined as anti-GSC-positive patients (anti-GSC(+) group) and grouped according to the specificity of the anti-GSC antibodies. We asked the attending physicians to provide detailed clinical data for those subjects for whom clinical information was insufficient. Patients without data concerning neurological signs and symptoms were excluded from the clinical analysis. Anti-GSC-negative patients with detailed clinical data formed the control group. Patients' disabilities were graded using the Hughes Functional Grading Scale (Hughes et al., 1978). Electrophysiological data were evaluated as described previously and categorized as "primary demyelinating," "primary axonal," "unexcitable," "equivocal," or "normal" (Hadden et al., 1998; Kaida et al., 2001). Clinical features and electrophysiological findings were compared between the anti-GSC(+) and control groups.

2.4. Investigations into the specificity of anti-ganglioside complex antibodies

To investigate the specificities of anti-GSC antibodies in anti-GSC antibody-positive serum samples, immunoabsorption and ELISA were performed using mixtures of more than two gangliosides. Anti-GSC antibodies were absorbed on antigen-coated ELISA wells as described previously (Kaida et al., 2001).

2.5. Statistical analysis

Differences in proportions were tested by the Fisher exact probability test or the χ^2 test. The Mann–Whitney test was used for comparisons of age, onset to nadir (days), and peak disabilities among the groups. Two-tailed p-values<0.05 were considered significant throughout. These analyses were performed with SPSS software (12.0, SPSS Inc., Chicago).

3. Results

3.1. Study population

We collected serum from 234 consecutive GBS patients including 100 patients previously published (Kaida et al., 2004). ELISA showed that 39 (17%) of these patients had IgG antibodies to at least one GSC such as GD1a/GD1b, GM1/GD1a, GD1b/GT1b, GM1/GT1b, or GM1/GD1b. Among the 39 anti-GSC-positive patients, all had IgG anti-GM1/GD1a antibodies and 27 had anti-GM1/GT1b antibodies. Sixteen patients had anti-GD1a/GD1b antibodies, 13 had anti-GD1b/GT1b antibodies, and six had anti-GM1/GD1b antibodies. Ten patients had both anti-GD1a/GD1b and anti-GD1b/GT1b antibodies. Distribution of anti-GSC(+) group patients was described with a Venn diagram (Fig. 1). No patients in either group had anti-GD1a/GT1b antibodies. Eight of the 39 anti-GSC-positive patients were already reported in the previous study (Kaida et al., 2004). There were no serum IgM antibodies to GSCs in any of the 39 patients. Representative ELISA results and TLC immunostaining are shown in Fig. 2. Specific immunostaining was found on the overlapping portions of each ganglioside (Fig. 2B). One in the Anti-GSC(+) group was excluded from the analysis of clinical features because detailed clinical data were unavailable. Twenty-five of the 195 anti-GSC-negative patients also were excluded because insufficient clinical data were available; the remaining 170 patients served as the control group.

3.2. Frequencies of antibodies to single ganglioside antigens

Thirty-four of 39 patients in the anti-GSC(+) group had antibodies to single gangliosides (Table 1). There were no significant differences in the frequency of antibodies to single ganglioside antigens between anti-GSC(+) and the control groups, except for IgG anti-GD1b antibody. One of eight ventilated patients in the anti-GSC(+) group had IgG anti-GQ1b antibody. Although the frequencies of IgG antibodies to GD1a, GD1b, or GT1b were significantly higher in three subgroups (Table 1), their OD values were much lower than those of anti-GSC antibodies (data not

Table 2
Clinical features of GBS patients in anti-GSC(+) and control groups

	Antibody specificity in anti-GSC(+) group*					
	GM1/GD1a (Anti-GSC(+))	GM1/GD1a GM1/GT1b	GM1/GD1a GM1/GT1b GD1a/GD1b	GM1/GD1a GM1/GT1b GD1b/GT1b	GM1/GD1a GM1/GT1b GD1a/GD1b GD1b/GT1b	Control
Clinical features	(n=38)	(n=27)	(n=16)	(n=13)	(n=10)	(n=170)
Age**	43.2 (37.7–48.8)	45.3 (38.0–52.6)	43.8 (34.4–53.1)	48 (35.8–60.2)	47.1 (33.2–61.0)	48.9 (45.6–52.1) (n=169)
Sex male/female	25/13	18/9	12/4	9/4	7/3	103/67
Antecedent infection						
Respiratory	19 (50%)	12 (44%)	4 (25%)	3 (23%)	2 (20%)	76 (45%)
Gastro-intestinal	17 (45%)[#1] (*C. jejuni*: 12)	14 (52%)[#2] (*C. jejuni*: 9)	12 (75%)[#3] (*C. jejuni*: 8)	10 (77%)[#4] (*C. jejuji*: 6)	8 (80%)[#5] (*C. jejuni*: 5)	38 (22%)
Onset to nadir (days)**	7.8 (6.1–9.6) (n=33)	7.8 (5.4–10.2) (n=24)	9.2 (4.8–13.6) (n=13)	9.7 (5.2–14.1) (n=12)	10.4 (4.3–16.6) (n=9)	7.8 (7.0–8.7) (n=158)
Cranial nerve deficits	(n=35)	(n=25)	(n=15)			(n=156)
positive	22 (63%)	18 (72%)	11 (73%)	10 (77%)	9 (90%)[#6]	80 (51%)
III, IV, VI	12 (34%)[#6]	11 (44%)[#2]	5 (33%)	6 (46%)[#2]	5 (50%)[#7]	25 (16%)
VII	11 (31%)	9 (36%)	7 (47%)	5 (38%)	5 (50%)	57 (37%)
IX, X	17 (49%)	15 (60%)[#8]	10 (67%)[#9]	9 (69%)[#10]	8 (80%)[#11]	48 (31%)
XI, XII	9 (26%)[#12]	7 (28%)[#10]	6 (40%)[#11]	5 (38%)[#9]	4 (40%)[#6]	13 (8.3%)
Sensory loss	9 (26%) (n=34)	9 (38%) (n=24)	5 (36%) (n=14)	5 (42%) (n=12)	5 (56%) (n=9)	61 (39%) (n=156)
Nerve conduction study	(n=26)	(n=18)	(n=9)	(n=7)	(n=6)	(n=46)
Demyelination	8 (31%)	5 (28%)	3 (33%)	2 (29%)	2 (33%)	18 (39%)
Axonal	6 (23%)	4 (22%)	3 (33%)	3 (43%)	2 (33%)	5 (11%)
Inexcitable	3 (12%)	3 (17%)	1 (11%)	1 (14%)	1 (17%)	4 (8.7%)
Artificial ventilation	8 (22%) (n=36)	7 (27%)[#13] (n=26)	6 (38%)[#9]	6 (46%)[#11]	5 (50%)[#14]	19 (11%)

* The Anti-GSC(+) group was divided into four subgroups based on antibody specficity of anti-GSC antibodies (see Fig 1). Anti-GM1/GD1b antibody-positive group is omitted in this table due to the small number of patients. ** mean (95% confidence interval) # indicates that there are significant differences between an antibody-positive group and remainder. Remainder include Control group patients and remaining anti-GSCantibody-positive patients. [#1], p=0.008; [#2], p=0.002, [#3], p<0.0001; [#4], p=0.0001; [#5], p=0.0005; [#6], p=0.02; [#7], p=0.03; [#8], p=0.006; [#9], p=0.009; [#10], p=0.01; [#11], p=0.003; [#12], p=0.007; [#13], p=0.03; [#14], p=0.004.

Table 3
Association of antibody specificities with peak disability

	Antibody specificity in anti-GSC(+) group					
	GM1/GD1a (Anti-GSC(+))	GM1/GD1a GM1/GT1b	GM1/GD1a GM1/GT1b GD1a/GD1b	GM1/GD1a GM1/GT1b GD1b/GT1b	GM1/GD1a GM1/GT1b GD1a/GD1b GD1b/GT1b	Control
Functional score	(n=36)	(n=26)	(n=16)	(n=13)	(n=10)	(n=170)
F-1	2 (5.6%)	1 (3.8%)	0 (0%)	0 (0%)	0 (0%)	6 (3.5%)
F-2	10 (28%)	7 (27%)	2 (13%)	3 (23%)	2 (20%)	48 (28%)
F-3	7 (19%)	3 (12%)	3 (19%)	1 (7.7%)	0 (0%)	42 (25%)
F-4	9 (25%)	8 (31%)	5 (31%)	3 (23%)	3 (30%)	54 (32%)
F-5	8 (22%)	7 (27%)	6 (38%)	6 (46%)	5 (50%)	19 (11%)
F-6	0 (0%)	0 (0%)	0 (0%)	0 (0%)	0 (0%)	1 (0.6%)
p value* (two-tailed)	0.63 vs. remainder** (n=170)	0.18 vs. remainder** (n=180)	0.008 vs. remainder** (n=190)	0.024 vs. remainder** (n=193)	0.012 vs. remainder** (n=196)	

*The Mann–Whitney test was used to compare functional score of two groups. **Remainder include Control group patients and remaining anti-GSC antibody-positive patients.

shown). TLC immunostaining using anti-GD1a/GD1b-positive sera showed no or little binding to GD1a or GD1b each, but intense binding to in the overlapping portion of GD1a and GD1b.

3.3. Antecedent *Campylobacter jejuni* infection in anti-ganglioside complex antibody-positive patients

Four patients in the anti-GSC(+) group had already been diagnosed as having antecedent *C. jejuni* enteritis at other hospitals. Of the remaining anti-GSC(+) group patients with antecedent gastrointestinal infection, eight were IgG anti-*C. jejuni* antibody-positive, one of whom was IgM anti-*C. jejuni* antibody-borderline. Overall, 12 Anti-GSC(+) group patients had antecedent *C. jejuni* enteritis (Table 2).

3.4. Clinical and electrophysiological features of anti-ganglioside complex-positive patients

Clinical features and electrophysiological findings in each group of patients are shown in Table 2. Results of statistical analysis of the clinical features are also shown in Table 2. Anti-GSC(+) group patients more frequently had antecedent gastrointestinal infections, ophthalmoplegia, and lower cranial nerve deficits. Among them, the anti-GD1a/GD1b or anti-GD1b/GT1b-positive patients had significantly higher F-scores at nadir and more frequently needed mechanical ventilation than the remaining subjects including control group patients (Table 3). Of 206 patients who had sufficient clinical data on peak disability, ventilated patients more frequently had IgG anti-GD1a/GD1b antibodies than unventilated ones (6/27, 22%, vs. 10/179, 5.6%) (two-tailed p value=0.009, odds ratio=4.85, χ^2 test). Anti-GD1b/GT1b antibodies also were more frequently found in ventilated patients (6/27, 22%, vs. 7/179, 3.9%) (two-tailed p value=0.003, odds ratio=7.02, χ^2 test). No patients required mechanical ventilation due to any respiratory disorder such as aspiration pneumonia.

In terms of the short-term outcome among patients with a peak F score of more than 2 and adequate follow-up data, improvement by one or more in the F score one month after the onset of GBS was found in 11 (65%) of 17 anti-GSC(+) group and 21 (68%) of 31 control group patients. In the anti-GSC(+) group patients, two (25%) of eight anti-GD1a/GD1b-positive patients and three (43%) of seven anti-GD1b/GT1b-positive patients improved by one or more in the F score one month after the onset of GBS. Anti-GD1a/GD1b-positive patients showed significantly poor recovery compared with the respective remainders (p=0.012, Fisher exact probability). There were no significant differences in treatment between the two groups (Table 4). In this study, because electrophysiological and clinical following-up data were insufficient to statistically compare between anti-GSC(+) and control groups, we could not confirm association of anti-GSC antibodies with electrophysiological results and poor outcome.

Table 4
Therapy in anti-GSC(+) and control groups

Treatment	Anti-GSC(+)	Control
	n=17	n=31
IVIG	10	17
PP	2	3
Combination (IVIG+PP)	3	3
Combination (IVIG+steroid)	2	4
Others	0	4*

IVIG = intravenous immunoglobulin.
PP = plasmapheresis, including plasma exchange and immunoadsorption therapy.
* Includes prednisolone (1), not done (2), and unknown (1) There were no significant differences in treatment between the two groups.

Table 5
Immunoabsorption study of anti-GSC antibodies with GSCs and single ganglioside antigens using serum from patient No.10

Antigens used for absorption[a]		Absorption rate			
		In anti-GD1a/GD1b antibody activity	In anti-GM1/GD1a antibody activity	In anti-GD1b/GT1b antibody activity	In anti-GM1/GT1b antibody activity
GSCs					
(−)	(Corrected OD)	0.48	0.60	0.67	0.92
GD1a/GD1b		100%	58%	76%	73%
GM1/GD1a		100%	100%	100%	100%
GD1b/GT1b		100%	57%	100%	72%
GM1/GT1b		100%	76%	81%	100%
Single ganglioside antigens					
(−)	(Corrected OD)	0.40	0.68	0.80	0.77
GM1		0%	0%	0%	0%
GD1a		35%	0%	37%	13%
GD1b		58%	5%	20%	11%
GT1b		0%	1%	14%	0%

GSCs = ganglioside complexes.
Uncoated wells served as controls. The serum from the patient No.10 was diluted 1:80 with 1% BSA in PBS.
[a] Each microtiter plate well was coated with a single ganglioside (0.25 μg) or a mixture of 0.2 μg of each ganglioside.

3.5. Immunoabsorption test

Immunoabsorption testing was done with serum from patient no.10 in the anti-GSC(+) group. The serum sample had IgG antibodies to GD1b (a corrected OD value was 0.16 when the serum was diluted 1:40) in addition to anti-GSC antibodies. Results of the immunoabsorption test are shown in Table 5. The serum antibodies reacted more specifically with GSCs than with single ganglioside antigens.

4. Discussion

The present study has shown that 17% of patients with GBS have IgG antibodies to at least one GSC such as GD1a/GD1b, GM1/GD1a, GD1b/GT1b, GM1/GT1b, and GM1/GD1b. The anti-GSC(+) group patients presented more frequently preceding gastrointestinal infection, ophthalmoplegia, and lower cranial nerve deficits than control group patients, although a selection bias in a control group may have influenced the results to some extent. A close association between the presence of anti-GD1a/GD1b and/or anti-GD1b/GT1b antibodies and a need for mechanical ventilation suggest that these antibodies may be useful predictors of a need for mechanical ventilation and a severe course of GBS.

A mixture of GM1 and a phospholipid such as phosphatidic acid, phosphatidylinositol, or phosphatidylserine, intensifies antiganglioside antibody activity in GBS serum (Kusunoki et al., 2003; Hirakawa et al., 2005). Anti-GM1 antibodies, however, appeared not to react with new epitopes generated by mixtures of phospholipids and GM1 because they had no activity toward phospholipids alone, whereas anti-GSC antibodies are likely to react with new epitopes in clustered gangliosides because of the weak activity toward individual ganglioside antigens. Anti-GSC(+) antibodies rarely bound toGM1/GD1b and never to GD1a/GT1b, suggesting that an epitope formed by a combination of [Galβ1–3GalNAc] and [NeuAcα2–3Galβ1–3GalNAc] in the terminal residues of gangliotetraose structures is important for the antibody binding (Fig. 3). When mixtures of three or four gangliosides (GM1, GD1a, GD1b, GT1b) were used as antigens in ELISA, anti-GSC antibody activity was often decreased (data not shown), supporting that epitopes targeted by anti-GSC antibodies are formed in a mixture of two gangliosides and have new specific conformations. We believe that a mixture of two gangliosides is an appropriate antigen for the surveillance of anti-GSC antibodies. The examination of serum antibodies to such complex antigens as GSCs may increase the spectrum of anti-ganglioside antibodies in GBS, enhancing their value as diagnostic markers.

Anti-GD1a/GD1b-and/or anti-GD1b/GT1b-positive patients were more likely to have a poor outcome and be

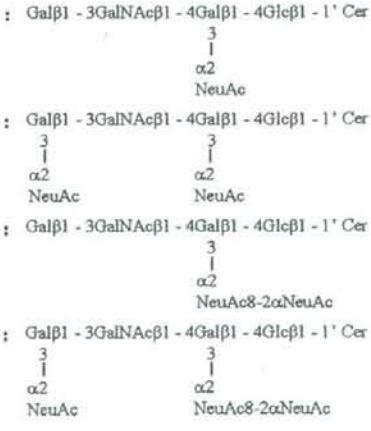

Fig. 3. Carbohydrate structures of GM1, GD1a, GD1b, and GT1b.

refractory to therapy than remaining subjects including control group patients, although more follow-up data are required to confirm the long-term prognosis. Why the anti-GD1a/GD1b-or anti-GD1b/GT1b-positive patients present a severe form of GBS is unclear. The different specificities of the anti-GSC antibodies might influence the peak disability and prognosis in anti-GSC antibody-positive patients. Most of anti-GD1a/GD1b-or anti-GD1b/GT1b-positive sera also react with GM1/GD1a and GM1/GT1b, suggesting that these sera are more multivalent than the antibodies reacting only with GM1/GD1a or GM1/GT1b, or with single ganglioside antigen. Tight binding between such multivalent antibodies and clustered glycoepitopes may correlate with a predisposition to a severe form of the disease.

Antecedent infection plays a critical role in the pathogenesis of GBS. Specific bacterial genes and ganglioside-mimicking structures in LOS of pathogens causing antecedent infection have proven to be essential for the induction of anti-ganglioside antibodies and determine antibody specificities (Ang et al., 2002; Yuki et al., 2004; Godschalk et al., 2004; Koga et al., 2005). Various ganglioside complex-like structures presumably exist in LOS of organisms causing antecedent infection. Cell wall glycoconjugates of *C. jejuni* might share epitopes with the GSCs such as GM1/GD1a or GD1a/GD1b, leading to the induction of anti-GSC antibodies.

Acknowledgments

We thank Miss Miwako Suemura for technical assistance, Dr. Yasuhisa Sakurai (Mitsui memorial hospital) for data collection, and Dr. Hiroshi Ashida (Division of Biomedical Information Sciences, National Defense Medical College Research Institute) for useful advice on the statistical analyses. We are grateful to the attendant physicians at the following hospitals for the collection of clinical data: Gunma University Hospital, Jichi Medical School Hospital, Jikei University Hospital, Nara Medical University Hospital, Nippon Medical School Hospital, Teikyo University Hospital, Tohoku University Hospital, Tokyo Women's Medical College Hospital, Tokyo University Hospital, Yamanashi University Hospital, Hiroshima Municipal Hospital, Kochi Municipal Central Hospital, Konan Hospital, Ronenbyo-Kenkyujo Hospital, Saiseikai Matsusaka General Hospital, Sendai Medical Center, Sendai Municipal Hospital, Showa General Hospital, Tokeidai Hospital, Toranomon Hospital, Toyohashi Hospital, Yamagata City Hospital Saiseikan.

This work was supported by the Ministry of Education, Culture, Sports, Science and Technology of Japan (Grants-in-Aid for Scientific Research, 16590854) and the Ministry of Health, Labour, and Welfare of Japan (Research Grant for Neuroinmunological Diseases and Health Sciences Research Grant on Psychiatric and Neurological Diseases and Mental Health, H15-015).

References

Ang, C.W., Laman, J.D., Willison, H.J., Wagner, E.R., Endtz, H.P., De Klerk, M.A., Tio-Gillen, A.P., Van den Braak, N., Jacobs, B.C., Van Doorn, P.A., 2002. Structures of *Campylobacter jejuni* lipopolysaccharides determines antiganglioside specificity and clinical features of Guillain–Barré syndrome and Miller Fisher patients. Infect. Immun. 70, 1202–1208.

Asbury, A.K., Cornblath, D.R., 1990. Assessment of current diagnostic criteria for Guillain–Barré syndrome. Ann. Neurol. 27, S21–S24 (Suppl).

Chiba, A., Kusunoki, S., Obata, H., Machinami, R., Kanazawa, I., 1993. Serum anti-GQ1b IgG antibody is associated with ophthalmoplegia in Miller Fisher syndrome and Guillain–Barré syndrome: clinical and immunohistochemical studies. Neurology 43, 1911–1917.

Godschalk, P.C.R., Heikema, A.P., Gilbert, M., Komagamine, T., Ang, C.W., Glerum, J., Brochu, D., Li, J., Yuki, N., Jacobs, B.C., van Belkum, A., Endtz, H.P., 2004. The crucial role of *Campylobacter jejuni* genes in anti-ganglioside antibody induction in Guillain–Barré syndrome. J. Clin. Invest. 114, 1659–1665.

Hadden, R.D.M., Cornblath, D.R., Hughes, R.A., Zielasek, J., Hartung, H.P., Toyka, K.V., Swan, A.V., 1998. Electrophysiological classification of Guillain–Barré syndrome: clinical associations and outcome. Plasma Exchange/Sandoglobulin Guillain–Barre Syndrome Trial Group. Ann. Neurol. 44, 780–788.

Hakomori, S., 2002. The glycosynapse. Proc. Natl. Acad. Sci. U. S. A. 99, 225–232.

Hirakawa, M., Morita, D., Tsuji, S., Kusunoki, S., 2005. Effects of phospholipids on antiganglioside antibody reactivity in GBS. J. Neuroimmunol. 159, 129–132.

Hughes, R., Newsom-Davis, J., Perkin, G., Pierce, J., 1978. Controlled trial of prednisolone in acute polyneuropathy. Lancet 2, 750–775.

Kaida, K., Kusunoki, S., Kamakura, K., Motoyoshi, K., Kanazawa, I., 2000. Guillain–Barré syndrome with antibody to a ganglioside, *N*-acetylgalactosaminyl GD1a. Brain 123, 116–124.

Kaida, K., Kusunoki, S., Kamakura, K., Motoyoshi, K., Kanazawa, I., 2001. Guillain–Barré syndrome with IgM antibody to the ganglioside GalNAc–GD1a. J. Neuroimmunol. 113, 260–267.

Kaida, K., Kusunoki, S., Kamakura, K., Motoyoshi, K., Kanazawa, I., 2003. GalNAc–GD1a in human peripheral nerve. Target sites of anti-ganglioside antibody. Neurology 61, 465–470.

Kaida, K., Morita, D., Kanzaki, M., Kamakura, K., Motoyoshi, K., Hirakawa, M., Kusunoki, S., 2004. Ganglioside complexes: as new target antigens in Guillain–Barré syndrome. Ann. Neurol. 56, 567–571.

Koga, M., Takahashi, M., Masuda, M., Hirata, K., Yuki, N., 2005. Campylobacter gene polymorphism as a determinant of clinical features of Guillain–Barre syndrome. Neurology 65, 1376–1381.

Kusunoki, S., Morita, D., Ohminami, S., Hitoshi, S., Kanazawa, I., 2003. Binding of immunoglobulin G antibodies in Guillain–Barré syndrome sera to a mixture of GM1 and a phospholipids: clinical implications. Muscle Nerve 27, 302–306.

Norgard, K.E., Moore, K.L., Diaz, S., Stults, N.L., Ushiyama, S., McEver, R.P., Cummings, R.D., Varki, A., 1993. Characterization of a specific ligand for P-selectin on myeloid cells. A minor glycoprotein with sialylated O-linked oligosaccharides. J. Biol. Chem. 268, 12764–12774.

Simons, K., Toomre, D., 2000. Lipid rafts and signal transduction. Nat. Rev., Mol. Cell Biol. 1, 31–39.

Varki, A., 1994. Selectin ligands. Proc. Natl. Acad. Sci. U. S. A. 91, 7390–7397.

Willison, H.J., Yuki, N., 2002. Peripheral neuropathies and anti-glycolipid antibodies. Brain 125, 2591–2625.

Yu, R.K., Iqbal, K., 1979. Sialosylgalactosyl ceramide as a specific marker for human myelin and oligodendroglial perikarya: gangliosides of human myelin, oligodendroglia and neurons. J. Neurochem. 32, 293–300.

Yuki, N., Susuki, K., Koga, M., Nishimoto, Y., Odaka, M., Hirata, K., Taguchi, K., Miyatake, T., Furukawa, K., Kobata, T., Yamada, M., 2004. Carbohydrate mimicry between human ganglioside GM1 and Campylobacter jejuni lipooligosaccharide causes Guillain–Barré syndrome. Proc. Natl. Acad. Sci. U. S. A. 101, 11404–11409.

Guillain–Barré syndrome with antibodies to GD1a/GD1b complex

Recently, ganglioside complexes (GSCs) such as GD1a/GD1b, GD1a/GM1, GD1b/GT1b, GM1/GT1b, GQ1b/GM1 and GQ1b/GD1a have been

shown as target antigens for serum antibodies in patients with Guillain–Barré syndrome (GBS)[1] and Miller Fisher syndrome (MFS).[2] Gangliosides may interact with each other to form a novel epitope, which serves as a target antigen for serum antibodies.[3] In particular, anti-GD1a/GD1b IgG is reported to be associated with severe GBS and requirement of mechanical ventilation.[3] However, there has been no previous case report describing GBS with anti-GSC antibodies in detail. In this report, we present a patient with GBS having anti-GD1a/GD1b antibody and investigated the clinical feature.

Case report

A 42-year-old man noticed weakness of the bilateral upper extremities 2 weeks after an episode of acute respiratory tract symptoms and diarrhoea. His symptoms further developed to dysarthria, dysphagia and tetraparesis, and he was admitted to the Department of Neurology, Ishikawa Prefecture Central Hospital, Kanazawa, Japan, 4 days after the onset of weakness. Neurological examination disclosed bilateral facial weakness, poor elevation of the soft palate, hoarseness, dysarthria, dysphagia, weakness of the tongue, flaccid tetraparesis (grade 4, Medical Research Council scale) and areflexia of deep tendon reflexes. He needed a wheelchair for transfer, and stomach tube for gastrogavage. Laboratory findings including cerebrospinal fluid (CSF) examination were normal, except for hypercapnia (P_{CO_2} 47.8 mm Hg) on blood gas analysis. Nerve conduction studies demonstrated a marked reduction of compound muscle action potentials (CMAP) with normal conduction velocity (CMAP was 2.87 mV and motor conduction velocity was 50.6 m/s in the right median nerve), but sensory nerves were normal. The MRI studies of the brain and spinal cord were normal. A diagnosis of GBS was made, and he was given intravenous immunoglobulin (IVIg; 400 mg/kg/day) and intravenous methylprednisolone (500 mg/day) for 5 days, according to the protocol used in the previously reported randomised trial.[4] He underwent rehabilitation, and his symptoms gradually improved 1 week after admission. He could stand by himself 2 weeks after admission, and eat by himself without a stomach tube 1 month after admission. Nerve conduction studies still showed simple reduction of CMAPs 1 month after admission (CMAP was 1.21 mV and motor conduction velocity was 53.0 m/s in the right median nerve). At 2 months after admission, he could ambulate independently. He returned to work (English teacher at a high school) 3 months after admission.

The antibodies to gangliosides (GM1, GM2, GM3, GD1a, GD1b, GD3, GT1b, GQ1b, GA1, Gal-C, and GalNac-GD1a) and GD1a/GD1b complex in the serum obtained on the first day of admission were examined by enzyme-linked immunosorbent assay, as previously described.[1 2] He was positive only to the antibody to GD1a/GD1b complex (anti-GD1a/GD1b antibody).

Comment

Our patient showed acute progressive axonal motor polyneuropathy involving the cranial nerves 2 weeks after flu-like symptoms. This condition fulfilled the established criteria of GBS, and the results of nerve conduction studies were classified as having acute motor axonal neuropathy (AMAN).[5] Anti-GD1a/GD1b antibody was detected in the acute-phase serum; however, there were no antibodies to single gangliosides, including GD1a and GD1b.

In a recent report,[3] 8 of 100 patients with GBS had anti-GD1a/GD1b antibodies, and three of these eight did not demonstrate any anti-ganglioside antibodies. These eight patients with anti-GD1a/GD1b antibody tended to have cranial nerve deficits and severe disabilities, and four of these patients required artificial ventilation.[3] Of the three anti-GD1a/GD1b antibody-positive patients with available electrophysiological data, two showed an axonal neuropathy pattern, and the remaining one showed an equivocal pattern.[3] Of the 12 patients with MFS, 7 had serum antibodies to some GSCs, and anti-GSC antibodies might influence the clinical features, as sensory signs were infrequent in patients with anti-GQ1b/GM1 antibody.[2] These findings may support the theory that anti-GSC antibodies correlate with a certain phenotype of GBS or MFS.

The clinical features of our patient were similar to those patients with anti-GD1a/GD1b antibodies,[3] such as AMAN-type GBS with cranial nerve deficits and severe disability (the Hughes Functional Grading Scale at the peak of his disability was on grade 4). Although our patient did not require artificial ventilation, his hypercapnia suggested respiratory weakness. The patient received intravenous methylpredonisolone in addition to IVIg. This combination therapy might prevent his case from being aggravated to grade 5. However, a future large-scale study will be needed to clarify this point.

Tsuyoshi Hamaguchi, Kenichi Sakajiri, Kenji Sakai, Soichi Okino
Department of Neurology, Ishikawa Prefecture Central Hospital, Kanazawa, Japan

Masami Sada, Susumu Kusunoki
Department of Neurology, Kinki University School of Medicine, Osaka-Sayama, Japan

Correspondence to: Dr T Hamaguchi, Department of Neurology, Ishikawa Prefecture Central Hospital, 2-1 Kuratsuki-higashi, Kanazawa 920-8530, Japan; gom56@ipch.jp

Informed consent was obtained for publication of the patient's details described in this report.

doi: 10.1136/jnnp.2006.108217

Competing interests: None declared.

References

1 **Kaida K**, Morita D, Kanzaki M, *et al*. Ganglioside complexes as new target antigens in Guillain–Barré syndrome. *Ann Neurol* 2004;**56**:567–71.
2 **Kaida K**, Kanzaki M, Morita D, *et al*. Anti-ganglioside complex antibodies in Miller Fisher syndrome. *J Neurol Neurosurg Psychiatry* 2006;**77**:1043–6.
3 **Van Koningsveld R**, Schmitz PIM, van der Meché, *et al*. Effect of methylprednisolone when added to standard treatment with intravenous immunoglobulin for Guillain–Barré syndrome: randomized trial. *Lancet* 2004;**363**:192–6.
4 **Kusunoki S**, Chiba A, Kon K, *et al*. N-acetylgalactosaminyl GD1a is a target molecule for serum antibody in Guillain–Barré syndrome. *Ann Neurol* 1994;**35**:570–6.
5 **Ho TW**, Mishu B, Li CY, *et al*. Guillain–Barré syndrome in northern China: relationship to Campylobacter jejuni infection and anti-ganglioside antibodies. *Brain* 1995;**118**:597–605.

Putaminal petechial haemorrhage as the cause of non-ketotic hyperglycaemic chorea: a neuropathological case correlated with MRI findings

Acute generalised chorea can be attributed to multiple causes, including non-ketotic hyperglycaemia. This cause has been associated with characteristic image signs of striatal hyperdensity on CT scan and hyperintensity on T1 weighted (T1W) MRI.

We report a patient presenting with this syndrome in which a postmortem study was conducted. The findings are discussed together with the neuropathological data available in the literature, contributing towards an explanation of the nature of the imaging signs that has remained elusive.

Case report

A 73-year-old woman was admitted to our neurological department for acute generalised chorea of 8 days' duration. There was no relevant personal background or family history.

On admission, the patient presented with orofacial dyskinesias and choreic movements in the neck, trunk, upper and lower limbs. The aetiological diagnostic work-up for acute chorea revealed severe hyperglycaemia on admission (>27.8 mmol/l), bicytopenia with anaemia (erythrocyte count 2.8×10^6/mm^3, haemoglobin 8.1 g/dl) and thrombocytopenia ($104\,000$/μl), and an isolated antiphospholipid antibody positive titre. The remaining investigation for acute chorea was normal. The imaging studies revealed a spontaneous bilateral hyperdensity in the putamen and caudate nuclei on the admission brain CT scan. The brain MRI (1.5T; Signa Horizon, General Elecrics Medical Systems, Milwaukee, Wisconsin, USA), conducted 2 weeks after admission, showed a bilateral putaminal hyperintensity in T1W images exclusively (fig 1).

Chorea persisted beyond glycaemia normalisation. The patient eventually died 32 days after admission as a result of unresolved sepsis, having begun with fever 4 days after admission. A postmortem examination was conducted.

In the neuropathological study, paraffin embedded representative sections of the left hemisphere, brainstem and cerebellum were stained with haematoxylin–eosin, Bodian–Luxol, Perls and Van Gieson stains. The basal ganglia region was studied using anterior and posterior coronal sections. Microscopic examination revealed generalised wall fibrosis of the small perforating arteries associated with dilatation of the perivascular spaces of the deep white matter. Multiple lacunes in the basal ganglia and thalamus were found in association with macrophage proliferation. Astrocytic gliosis and extravascular hemosiderin deposits together with ferruginateous deposits on perforating vessels were observed in the posterior zone of the putamen. No vascular amyloid or calcium deposits were observed.

Discussion

In our case, the triad of acute chorea, non-ketotic hyperglycaemia and a hyperdense and hyperintense putamen on CT and T1W MRI was documented. The bicytopenia and an antiphospholipid antibody positive titre could

Molecular Biology of the Cell
Vol. 18, 2112–2122, June 2007

Gangliosides GM1 and GM3 in the Living Cell Membrane Form Clusters Susceptible to Cholesterol Depletion and Chilling[D]

Akikazu Fujita,* Jinglei Cheng,* Minako Hirakawa,† Koichi Furukawa,‡ Susumu Kusunoki,† and Toyoshi Fujimoto*

Departments of *Anatomy and Molecular Cell Biology and ‡Biochemistry II, Nagoya University Graduate School of Medicine, Nagoya 466-8550, Japan; and †Department of Neurology, Kinki University School of Medicine, Osaka 589-8511, Japan

Submitted January 26, 2007; Revised March 6, 2007; Accepted March 20, 2007
Monitoring Editor: Jean Gruenberg

Presence of microdomains has been postulated in the cell membrane, but two-dimensional distribution of lipid molecules has been difficult to determine in the submicrometer scale. In the present paper, we examined the distribution of gangliosides GM1 and GM3, putative raft molecules in the cell membrane, by immunoelectron microscopy using quick-frozen and freeze-fractured specimens. This method physically immobilized molecules in situ and thus minimized the possibility of artifactual perturbation. By point pattern analysis of immunogold labeling, GM1 was shown to make clusters of <100 nm in diameter in normal mouse fibroblasts. GM1-null fibroblasts were not labeled, but developed a similar clustered pattern when GM1 was administered. On cholesterol depletion or chilling, the clustering of both endogenous and exogenously-loaded GM1 decreased significantly, but the distribution showed marked regional heterogeneity in the cells. GM3 also showed cholesterol-dependent clustering, and although clusters of GM1 and GM3 were found to occasionally coincide, these aggregates were separated in most cases, suggesting the presence of heterogeneous microdomains. The present method enabled to capture the molecular distribution of lipids in the cell membrane, and demonstrated that GM1 and GM3 form clusters that are susceptible to cholesterol depletion and chilling.

INTRODUCTION

Microdomains enriched with cholesterol and sphingolipids, or rafts, have been postulated to exist in the cell membrane (Simons and Ikonen, 1997). Domains showing a liquid-ordered state have been visualized in model membranes (Korlach *et al.*, 1999; Dietrich *et al.*, 2001a), but whether similar domains exist in the biological membranes of living cells, and what their basic properties would be, including size, life span and dynamics, are still under debate (Simons and Ikonen, 1997; Edidin, 2003; Munro, 2003; Kusumi *et al.*, 2004; Mayor and Rao, 2004; Mukherjee and Maxfield, 2004). Recent results, obtained by single-particle tracking and fluorescent resonance energy transfer experiments, have suggested that rafts in normal unstimulated cells are extremely small and may last for <1 ms (Kenworthy *et al.*, 2004; Kusumi *et al.*, 2004; Sharma *et al.*, 2004). Detergent-resistant membranes have often been regarded as an in vitro correlate of rafts, but detergents themselves have been found to cause domain formation artificially (Heerklotz, 2002). These results have thus posed questions regarding the true existence of rafts in living, nonstimulated cells. In addition, although microscopic identification of rafts has been attempted in a number of studies, putative raft molecules generally show diffuse distribution in the cell membrane without any concentration at the resolution of light microscopy. This result has been interpreted in several different ways, i.e., that rafts do not in fact exist, rafts are too small to be resolved by light microscopy, rafts occupy the majority of the membrane, or rafts do exist but may be disrupted by experimental procedures.

GM1 has been generally regarded as an authentic raft molecule, and cholera toxin B-subunit (CtxB) has been used to probe its distribution in many microscopic studies including FRET (Kenworthy *et al.*, 2000; Nichols, 2003). However, because CtxB is a pentameric molecule that can bind to five GM1 molecules, binding of CtxB itself is likely to change the distribution of GM1 in the membrane as shown for membrane proteins that were cross-linked with antibodies (Mayor *et al.*, 1994; Fujimoto, 1996). Some studies used specimens that were fixed before the CtxB labeling (Parton, 1994), but chemical fixatives are unlikely to preserve the in situ localization of membrane molecules, particularly lipids, and may even cause artifactual results (Jost *et al.*, 1973; Chandler, 1984).

This article was published online ahead of print in *MBC in Press* (http://www.molbiolcell.org/cgi/doi/10.1091/mbc.E07-01-0071) on March 28, 2007.

[D] The online version of this article contains supplemental material at *MBC Online* (http://www.molbiolcell.org).

Address correspondence to: Toyoshi Fujimoto (tfujimot@med.nagoya-u.ac.jp).

Abbreviations used: b-CtxB, biotinylated cholera toxin B; CI, confidence interval; CSR, complete spatial randomness; EM, electron microscopy; GAR-Fab5, colloidal gold (5-nm)-conjugated anti-rabbit IgG F(ab')2 fragment; PAG5, colloidal gold (5-nm)-conjugated protein A; MβCD, methyl-β-cyclodextrin; NND, nearest neighbor distance; PC, phosphatidylcholine; SDS-FRL, SDS-treated freeze-fracture replicas.

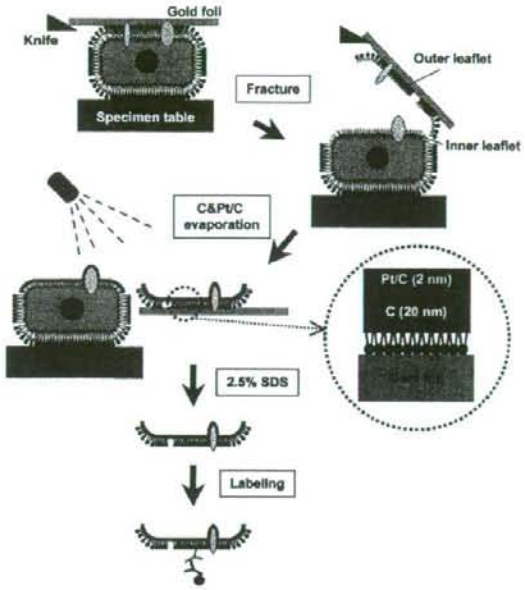

Figure 1. Outline of the SDS-FRL technique used in the present study. Cells cultured on thin gold foils were quick-frozen and freeze-fractured. Replicas were made by evaporation of carbon followed by platinum/carbon in most experiments. The replicas were treated with SDS and labeled with antibodies.

To avoid the possible artifacts caused by probe binding and chemical fixation, and also to take advantage of the high resolving power of electron microscopy (EM), we turned to immuno-EM using SDS-treated freeze-fracture replicas (SDS-FRL) (Figure 1). In combination with rapid freezing, SDS-FRL can immobilize membrane molecules physically and determine their localization in the nanometer range (Fujimoto, 1995). By use of this method, we wanted to examine whether putative raft lipids are distributed in clusters in the living cell membrane as postulated in the raft hypothesis.

In the present study, we labeled gangliosides GM1 and GM3 in the mouse fibroblast membrane, and we analyzed the result by spatial statistical methods in wide membrane areas. As a result, both GM1 and GM3 were found to form clusters in normal mouse fibroblasts, and their clustering became less obvious after cholesterol depletion. Contrary to the simplest raft hypothesis, dissolution of the cluster upon cholesterol depletion was not complete, and it showed regional heterogeneity; and, unexpectedly, a similar result was observed when cells were cooled on ice before rapid freezing. Additionally, clusters of GM1 and GM3 overlapped only partially, suggesting the presence of heterogeneous microdomains. These observations were discussed with reference to the findings obtained using other methodologies.

MATERIALS AND METHODS

Antibodies and Probes

Rabbit anti-GM1 antibodies were raised and affinity-purified as described previously (Kusunoki *et al.*, 1996). Two different batches of antibodies were used in the present study, and they gave equivalent results. Mouse anti-GM3 antibody (clone GMR6; Seikagaku-Kogyo, Tokyo, Japan) and biotin-conjugated cholera toxin B-subunit (b-CtxB; Invitrogen, Carlsbad, CA) were purchased. Mouse anti-phosphatidylcholine (PC) antibody (JE-1) (Nam *et al.*, 1990) was kindly donated by Dr. Masato Umeda (Kyoto University). Secondary antibodies conjugated with fluorochromes (Invitrogen), horseradish peroxidase (Pierce Chemical, Rockford, IL), and colloidal gold (BioCell, Cardiff, United Kingdom), and protein A coupled to colloidal gold (University Medical Center Utrecht, Utrecht, The Netherlands) were obtained from respective suppliers.

Cells

Fibroblasts were explanted from the dermis of wild-type mice and mice lacking the β1,4-*N*-acetylgalactosamine-transferase gene (Takamiya *et al.*, 1996). They were maintained in DMEM supplemented with 10% fetal calf serum, 50 U/ml penicillin, and 0.05 mg/ml streptomycin at 37°C under 5% CO_2, 95% air. The latter cells were referred to as GM1-null fibroblasts. To load GM1-null cells with exogenous GM1 (Sigma-Aldrich, St. Louis, MO), the cells were incubated in serum-free DMEM containing GM1 (0.3, 3, or 30 μM) for 1 h at 37°C in the CO_2 incubator. After incubation, the cells were washed twice with phosphate-buffered saline (PBS) and incubated with PBS containing 0.2% fatty acid-free bovine serum albumin (BSA) (Wako Pure Chemicals, Osaka, Japan) to remove GM1 loosely bound to the cell surface (Schwarzmann *et al.*, 1983). For cholesterol depletion, cells were treated with 5 mM methyl-β-cyclodextrin (MβCD) in DMEM for 60 min.

Thin-Layer Chromatography (TLC) Immunoblotting and Dot Blotting

Total lipids were extracted from cells by using chloroform/methanol, and glycosphingolipids were obtained by reverse phase chromatography with Sep-Pak C18 cartridge (Waters, Milford, MA) (Williams and McCluer, 1980). TLC was performed with high-performance TLC plates (Merck, Darmstadt, Germany) with a solvent system of chloroform/methanol/0.25% $CaCl_2$ (60: 35:8). For staining by resorcinol, 0.5 μg of gangliosides was loaded. For TLC immunoblotting, 0.25 μg of gangliosides was developed on TLC plates, transferred to polyvinylidene difluoride membranes, and immunolabeled as described previously (Taki and Ishikawa, 1997). For dot blotting, glycosphingolipids were blotted on the nitrocellulose membrane. The signals of blotting were detected using the SuperSignal West Dura Extended Substrate (Pierce Chemical) according to the manufacturer's instruction.

Immunofluorescence Microscopy

Cells cultured on glass coverslips were fixed with buffered 4% formaldehyde, pretreated with 3% BSA, and incubated with antibodies or b-CtxB, followed by the fluorochrome-conjugated secondary reagents. In some experiments, unfixed cells were incubated with the primary probes on ice, fixed, and then labeled by the secondary reagents. The labeled samples were observed by an Axiophot2 microscope (Carl Zeiss, Jena, Germany) equipped with an AxioCam charge-coupled device camera using an Apochromat oil immersion 63× objective lens with a numerical aperture of 1.4. For quantification of filipin labeling intensity, focus was adjusted by rhodamine-phalloidin in the same specimen, and filipin fluorescence was pictured without observation by an identical microscope setting, and analyzed by ImageJ (National Institute of Health, Bethesda, MD).

Quick-Freezing and Freeze-Fracture

Cells grown on a small gold foil (~4 mm^2 in area, 20 μm in thickness) were inverted upon prewarmed 10% gelatin on a gold-plated copper specimen table with the cell side down according to the metal sandwich method (Fujimoto and Fujimoto, 1997). The cell sandwich was slammed onto the copper block precooled to the liquid helium temperature (−269°C) by using the rapid freezing apparatus HIF-4K (Hitachi High-Technologies, Tokyo, Japan).

For freeze-fracturing, the specimens were transferred to a cold stage of a Balzers BAF400 apparatus, and they were fractured at −95°C and ~2×10^{-6} mbar. Replicas of the fractured membrane were made by electron-beam evaporation of platinum/carbon (Pt/C) and carbon (C), and the replica thickness was controlled by a crystal thickness monitor. Three different evaporation protocols were tested: 1) Pt/C (2 nm) followed by C (20 nm), 2) C (20 nm) followed by Pt/C (2 nm), 3) C (2 nm) followed by Pt/C (2 nm), and then by C (20 nm). After thawing, the replicas were immediately treated for 5 min in 2.5% SDS in PBS at 70°C. They were adjusted to 50% glycerol and kept at −20°C until labeling. Immunogold labeling was done as described previously (Fujimoto *et al.*, 1996), and the specimens were observed with a JEOL 1200EX electron microscope operated at 100 kV.

Statistical Analysis of Immunogold Labeling

Electron micrographs were digitized with an image scanner. The *x*-*y* coordinates of gold particles were obtained by Image Processing Tool Kit version 5 plug-in (Reindeer Graphics, Asheville, NC) for Adobe Photoshop version 6 (Adobe system, Mountain View, CA), and areas of 1 μm × 1 μm chosen randomly were analyzed by Ripley's K-function (Ripley, 1979) by using a program provided by John Hancock (Prior *et al.*, 2003). For significance tests,

99% confidence envelopes for complete spatial randomness (CSR) were generated from 100 Monte Carlo simulations. The frequency distribution of the nearest neighbor distance distribution was obtained by using the Image Processing Tool Kit.

Measurement of Phospholipids Bound to Replicas

The amount of phospholipids retained in SDS-treated C-Pt/C replicas was measured as described previously. Briefly, a suspension of small unilamellar PC liposomes was sandwiched between two thin copper foils, quickly frozen, freeze-fractured, and shadowed. One of the complementary replicas was washed in distilled water, and the other replica was treated with 2.5% SDS and washed with distilled water. The replicas were treated with 70% perchloric acid at 200°C for 2 h, and the released phosphorus was measured (Zhou and Arthur, 1992).

Biochemical Assay of Cholesterol

The total lipids were extracted from cells by a mixture of hexane and isopropanol (3:2), and the amount of free cholesterol was measured by enzymatic fluorometric method as described previously (Heider and Boyett, 1978).

On-Grid Model Experiment

Colloidal gold (2 nm; BioCell) conjugated with recombinant glutathione S-transferase (GST) was applied to Formvar-coated EM grids, blocked, and labeled with rabbit anti-GST followed by GAR-Fab5 or by PAG5. In other experiments, a dilute solution of recombinant GST was put on Formvar-coated grids and labeled by the same protocol.

RESULTS

Antibody Specificity

In enzyme-linked immunosorbent assay analysis with purified gangliosides, one of the two rabbit anti-GM1 antibodies used in our present study reacted with GM1 alone, whereas the other one also bound to GD1b and GA1. However, neither of these GM1 antibodies recognized GM2, GM3, GD1a, GD3, or GT1b (data not shown). In addition, by TLC blotting of gangliosides extracted from mouse fibroblasts, both of these antibodies showed positive reactivity only at the GM1 position and not GD1b or GA1 (Supplemental Figure 1). b-CtxB also reacted at the same position as the anti-GM1 antibodies. The monoclonal anti-GM3 antibody produced a band in cell extracts at the correct GM3 position and not GM1 (Supplemental Figure 1). The bands recognized by anti-GM1 and anti-GM3 antibodies were broader in the cell samples than that were for purified GM1 and GM3 molecules, but this is probably due to the presence of heterogeneous fatty acids, and/or the presence of glycolyl and acetylated forms of sialic acids in fibroblasts.

Immunogold Labeling of Freeze-Fracture Replicas

We previously showed that phospholipids are retained on SDS-treated freeze-fracture replicas and that they can be labeled by antibodies, but the labeling density was relatively low (Fujimoto *et al.*, 1996). To explore different conditions that may facilitate the efficient labeling of GM1, we compared replicas prepared in three different ways. In replicas produced by the conventional evaporation method, e.g., Pt/C (2 nm) followed by C (20 nm), labeling was found to be extremely low either by anti-GM1 antibody or by b-CtxB. The labeling intensity was improved, however, when the replicas were prepared by evaporating C before Pt/C. C (20 nm)-Pt/C (2 nm) replicas and C (2 nm)-Pt/C (2 nm)-C (20 nm) replicas gave equivalent results (Supplemental Figure 2). The retention of phospholipids in the SDS-treated replicas was not compromised by the change of the evaporation method: 82.6 ± 13.0% (n = 3) phosphatidylcholine was retained in the C (20 nm)-Pt/C (2 nm) replicas, which was even better than the retention ratio obtained for the conventional Pt/C (2 nm)-C (20 nm) replicas (Fujimoto *et al.*, 1996). Although the structural details became somewhat less defined in the C (20 nm)-Pt/C (2 nm) replica, we adopted this method in the present study due to its simplicity. Regardless of the procedure that was used for replica preparation, the labeling of GM1 was observed only in the E face, which represents the outer leaflet, and not in the P face, which represents the inner leaflet, or in the cytoplasm (Figure 3A, inset). Because the rabbit anti-GM1 antibodies gave significantly better labeling than b-CtxB, we used these antibodies in all of the subsequent EM experiments. The labeling efficiency of GM1 by the current method was calculated as described in Supplemental Table 1, and it was estimated that no less than 19.4% of GM1 in the original membrane was captured by immunogold labeling on the replicas.

The specificity of labeling in the replicas was confirmed using GM1-null cells (Takamiya *et al.*, 1996). Replicas of those cells were devoid of labeling either by the anti-GM1 antibodies or by b-CtxB (Figure 2C). Significantly, however, positive labeling by both probes was observed when exogenous GM1 was added to the culture medium before freezing. The quantitative loading of GM1 was confirmed by dot blotting and immunofluorescence microscopy (Figure 2, A and B), and the density of replica labeling increased as the GM1 concentration in the medium was raised from 0.3 to 30 μM (Figure 2C). The distribution of the labeling in the GM1-loaded cells was indistinguishable from that in normal mouse fibroblasts. Detailed analysis of the labeling is described below. Because the current methodology precludes the observation of molecules outside the lipid bilayer, the aforementioned results also demonstrate that exogenous GM1 molecules are incorporated into the cell membrane and that they adopt a similar disposition to endogenous GM1.

Distribution of GM1 in the Cell Membrane

By use of the aforementioned technique, GM1 distribution in normal mouse fibroblasts was examined. Immunogold labeling gave apparently clustered distribution (Figure 3A). To obtain objective data, 50 areas of 1 × 1 μm were randomly chosen from samples obtained in more than three independent experiments, and the distribution patterns were assessed by point pattern analysis using Ripley's K-function (Ripley, 1977, 1979; Prior *et al.*, 2003). When all the samples were compiled, the $L(r) - r$ curve was found to deviate most from the 99% confidence interval (CI) at a radius of 47.0 nm (Figure 3B). When individual samples were analyzed, the $L(r) - r$ curve showed a prominent peak except in a few cases (Supplemental Figure 3), and the peak size ranged from 32 to 68 nm (Figure 3C). We assumed that the basic cluster is in this size range (the size includes the arm length of the antibodies, which will be discussed later), and in subsequent experiments we classified the GM1 distribution patterns as "clustered" when the K-function was above the 99% CI at more than one point below a 100-nm radius. By this criterion, the GM1 labeling was clustered in all of the randomly chosen areas (50/50). The density of immunogold particles per unit area was found to be quite variable (Figure 4F), but GM1 clustering was observed irrespective of the labeling density.

The aforementioned result was obtained using rabbit anti-GM1 as the primary antibody, and colloidal gold (5 nm)-conjugated anti-rabbit IgG F(ab')2 fragment (GAR-Fab5) as the secondary probe. Because of the small size of the GM1 head group and the highly selective binding characteristics of the anti-GM1 antibody, it is unlikely that more than two primary antibodies bound to a GM1 molecule. In contrast, more than two GAR-Fab5 particles could bind to a primary antibody. However, we concluded that the clustering of GM1 labeling was not due to multivalency based on the

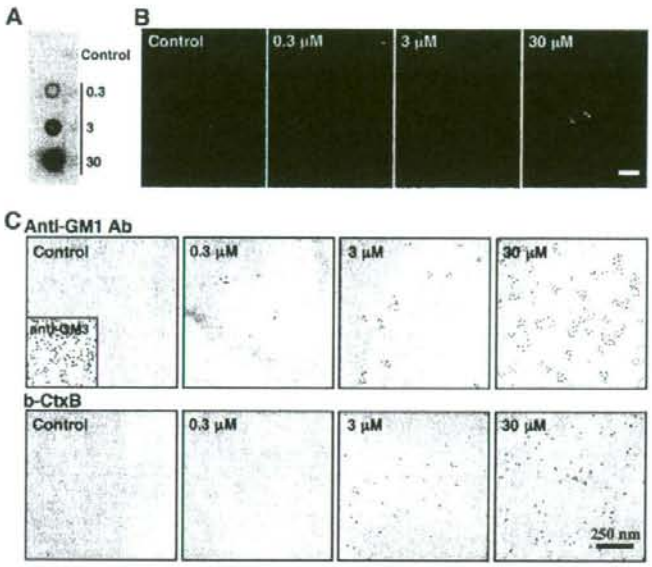

Figure 2. Fibroblasts obtained from GM1-null mice were cultured with or without 0.3, 3, or 30 μM GM1 for 60 min. (A) Dot blot labeling by b-CtxB. (B) Fluorescence microscopy using b-CtxB, followed by fluorescein isothiocyanate-avidin. The addition of GM1 to the culture medium increases the GM1 content in GM1-null mouse fibroblasts. Scale bar, 10 μm. (C) Freeze-fracture replicas were labeled by anti-GM1 antibody (top row), or by b-CtxB (bottom row). With either probe, labeling was not observed without GM1 loading, and labeling increased according to the amount of loading. Labeling of GM3 was observed without GM1 loading (inset). Ten-nanometer colloidal gold was used for labeling.

following results. First, a model experiment showed that two or three GAR-Fab5 particles could bind to an IgG molecule in 15.7 and 3.6% of the cases, respectively. When random point patterns were generated and the above-mentioned proportions of points were duplicated or triplicated, however, the resultant patterns did not show clustering as analyzed by Ripley's K-function (Supplemental Figure 4). Second, a very similar clustering was obtained when using colloidal gold (5 nm)-conjugated protein A (PAG5) as the secondary probe (Supplemental Figure 5, A and B). Only one PAG5 particle should bind to an IgG molecule, and the result of the model experiment was consistent with this principle (Supplemental Figure 4).

We next analyzed the entire area of randomly chosen cells to examine possible local heterogeneity within a single cell. Replicas were often disrupted within the cellular boundary, but areas of 145 μm^2 (ranging from 55 to 327 μm^2) could be observed on average for each cell. From this analysis, 70% of the cells showed only a clustered distribution throughout their surface, but the remainder showed small areas of random distribution (Figure 4D). An example of a whole cell profile and local $L(r) - r$ curves is shown in Supplemental Figure 6.

Effects of Cholesterol Depletion and Low Temperatures on GM1 Clustering

We next examined distribution of GM1 in mouse fibroblasts after depleting cholesterol to disrupt rafts. In cells treated with 5 mM MβCD for 60 min, the free cholesterol content was reduced considerably (Supplemental Figure 7). In these cells, 28% (14/50) of the areas showed random GM1 distribution, but 72% (36/50) still showed clustering (Figure 4C). Essentially, the same result was obtained when PAG5 was used for labeling (Supplemental Figure 5, B and C). Analysis of the compiled data also showed clustering (Figure 4A), but when individual samples were assessed, the peak of the $L(r) - r$ curves was clearly lower, broader, and less distinct compared with the control sample (Supplemental Figure 3).

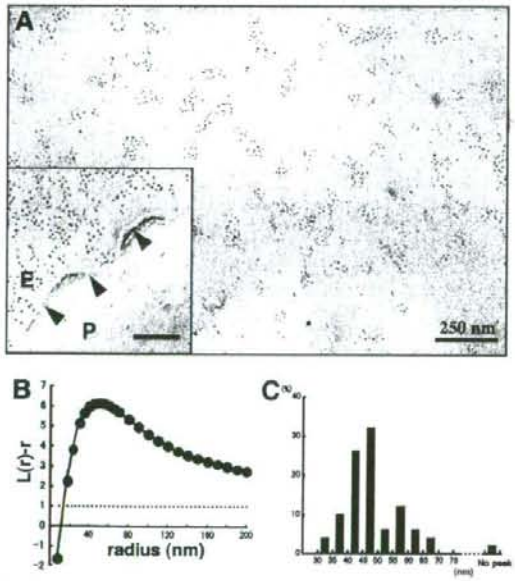

Figure 3. Labeling of freeze-fracture replicas of normal mouse fibroblasts by rabbit anti-GM1 antibody and colloidal gold (5-nm)-conjugated anti-rabbit IgG F(ab')2 fragment (GAR-Fab5). (A) GM1 labeling by 5-nm colloidal gold particles was detectable as clusters in the E face of the freeze-fractured plasma membrane. Inset, the P face was unlabeled. The cell boundary is marked by arrowheads. Ten-nanometer colloidal gold was used for labeling in this sample. (B) Fifty areas (1 × 1 μm) were randomly photographed, and the gold point patterns were analyzed by Ripley's K-function. The mean $L(r) - r$ curve showed maximal deflection from CSR (99% CI is shown by a dotted line) at a 47.0-nm radius. (C) Radii of maximal deflection for 50 sample areas ranging from 32 to 68 nm, with only one area showing no apparent peak.

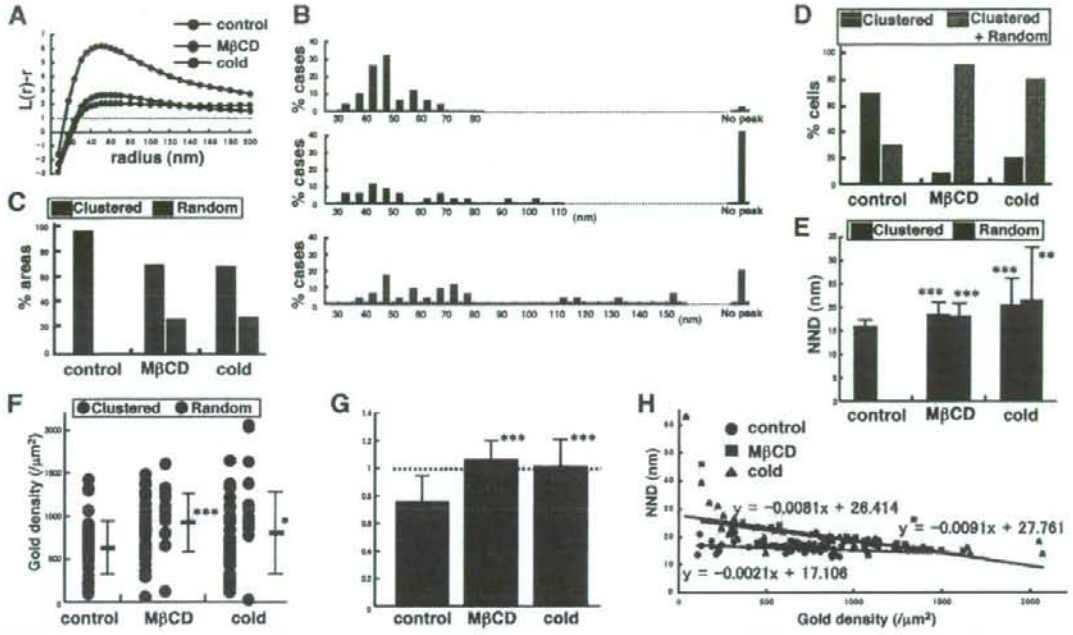

Figure 4. Analysis of GM1 distribution in normal mouse fibroblasts under three different conditions: control, cholesterol depletion, and incubation on ice for 30 min. (A) Mean $L(r) - r$ curves. The pooled data show clustering even after cholesterol depletion or chilling, but deviation from CSR was considerably smaller than the control. (B) Radii of maximal deflection in 50 areas. $L(r) - r$ curves without any peak below $r = 200$ nm increased after either treatment. (C) Classification based on K-function analysis. Areas showing more than one point above the 99% CI below $r = 100$ nm were regarded as clustered. (D) Classification of 10 randomly chosen cells. The entire area in each cell was analyzed. Cells were classified by whether they showed clustered areas only or both clustered and random areas. (E) NND analysis. NND values increased significantly after cholesterol depletion or chilling, compared with control cells (Student's t test; $^{**}p < 0.005$, $^{***}p < 0.001$). (F) The average labeling density showed a wide range for each sample and increased significantly after cholesterol depletion or chilling (Student's t test; $^{*}p < 0.05$, $^{***}p < 0.001$). (G) NND normalized to the value expected for random distribution. Only the control sample showed a value significantly <1 ($^{***}p < 0.001$). (H) Correlation of NND and the average labeling density. The dependence of NND upon the labeling density was far less in the control than in the treated samples.

In cholesterol-depleted wild-type mouse fibroblasts, the clustered and random distribution patterns of GM1 coexisted in >90% of the cells (Figure 4D). As shown in representative cases (Figure 5 and Supplemental Figure 6), the two different patterns were often observed side by side in narrow areas of the membrane. The result confirmed that the clustering of GM1 was not caused artifactually by the experimental procedures after freezing.

With the assumption that a low temperature would increase the raft area, and thus induce a further GM1 clustering, we kept mouse fibroblasts on ice for 30 min before rapid freezing. In contrast to the assumption, however, the distribution of the GM1 labeling in those cells showed changes that were very similar to those observed in cholesterol-depleted cells. The areas showing both clustered and random GM1 patterns were 70% (35/50) and 30% (15/50), respectively (Figure 4C). Individual samples also revealed a similar tendency, and the $L(r) - r$ curves generally became less distinct and broader than the control (Supplemental Figure 3). The coexistence of both clustered and random distribution patterns of GM1 in these cells was also observed in 80% of cases (Figure 4D). The changes caused by the cold were not likely to be caused by energy depletion because treatment with 10 mM sodium azide and 10 mM 2-deoxyglucose for 30 min, which inhibited endocytosis of CtxB completely, did not affect the GM1 distribution (data not shown).

Cholesterol depletion and low temperatures caused similar changes in two other indices: both the nearest neighbor distance (NND) and the average labeling density values increased significantly (Figure 4, E and F). The average NND, normalized to the value expected for random distribution, was significantly <1 in the control cells, but it became close to 1 after either cholesterol depletion or chilling (Figure 4G). Most significantly, the NND was virtually independent of the labeling density in control cells, whereas the NND decreased as the labeling density increased in cells after cholesterol depletion or chilling (Figure 4H). These data strongly indicate that GM1 in control mouse fibroblasts is clustered and that it becomes less so after cholesterol depletion or chilling.

The changes caused by cholesterol depletion and the cold were observed similarly in GM1-null cells preloaded with 10–15 μM GM1. The peak of the $L(r) - r$ curves became lower (Figure 6A), the frequency of random areas increased (Figure 6B), and the average labeling density increased (Figure 6C). Cholesterol depletion caused a more drastic change in the GM1-loaded cells than in the normal mouse fibroblasts. The reason is not clear, but some difference in the fatty acid composition between exogenous GM1 derived

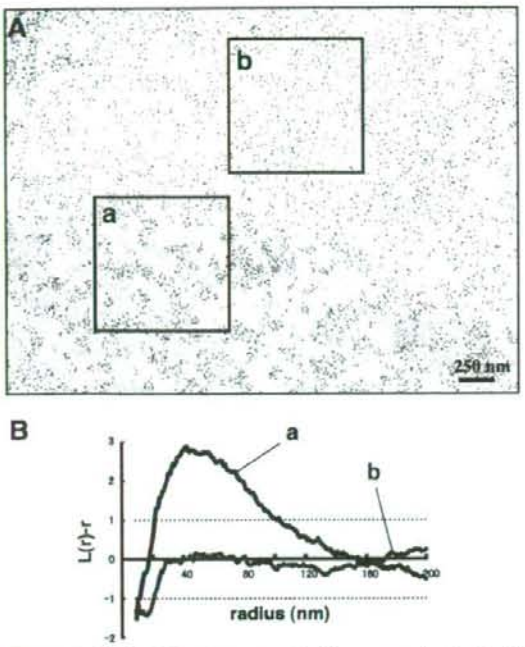

Figure 5. GM1 labeling in mouse fibroblasts treated with 5 mM MβCD for 60 min. (A) The labeling shows a marked regional heterogeneity in most cells. (B) The gold point patterns of adjacent areas in A show clustered (a) and random (b) distributions, respectively.

from bovine brain and GM1 expressed endogenously in mouse fibroblasts may be involved.

As a control, PC was labeled by SDS-FRL. Probably because the epitope of the anti-PC antibody includes a hydrophobic portion of PC that is located deeper in the lipid bilayer (Nam *et al.*, 1990), the antibody can only bind to a certain population of PC molecules, and the labeling does not occur homogenously even on liposome replicas (see figure 2A of Fujimoto *et al.*, 1996). A similar patchy labeling pattern was observed in the mouse fibroblast (Figure 7A). In contrast to GM1 (Figure 3) and GM3 (see below), the distribution of the PC labeling was not affected by cholesterol depletion, whereas chilling caused reduction of clustering (Figure 7B). Because of the unidentified binding characteristics of the anti-PC antibody, definite interpretation of the result is not possible, but the result showed that the distributional changes do not occur in the same manner in membrane lipids.

Distribution of GM3 in Relation to GM1

We next examined distribution of another ganglioside, GM3, by the same technique. GM3 also showed a clustered pattern in normal mouse fibroblasts (Figure 8). In comparison with GM1, the $L(r) - r$ curve of the GM3 labeling did not show an evident peak (Figure 8A), indicating that the size of the GM3 cluster was highly variable and generally larger than that of the GM1 cluster. We confirmed that the indirect immunolabeling protocol, i.e., mouse immunoglobulin M (IgM) followed by colloidal gold-conjugated anti-mouse Ig antibody, did not cause prominent clustering by a model experiment similar to Supplemental Figure 4 (data not shown). In cells depleted of cholesterol by MβCD, the clustering of GM3 decreased significantly (Figure 8B). According to the criterion used for GM1, 26.7% (8/30) of the area showed random distribution, and in the rest of the cases, the $L(r) - r$ curve was out of the CI range (Figure 8C). But as in the case of GM1, analysis of the individual areas showed that the $L(r) - r$ curves became generally lower in cholesterol-depleted cells even when they were classified as "clustered" by the criterion used for GM1 (Supplemental Figure 8). These results indicated that the clustering of GM3 is also related to the cholesterol content of the plasma membrane.

The relationship between the GM1 and GM3 clusters in normal mouse fibroblasts was examined by double labeling by using colloidal gold particles of two different diameters. By use of the bivariate K-function, two different patterns were observed. In a relatively limited number of areas (13.3%), GM1 and GM3 were observed to make coclusters,

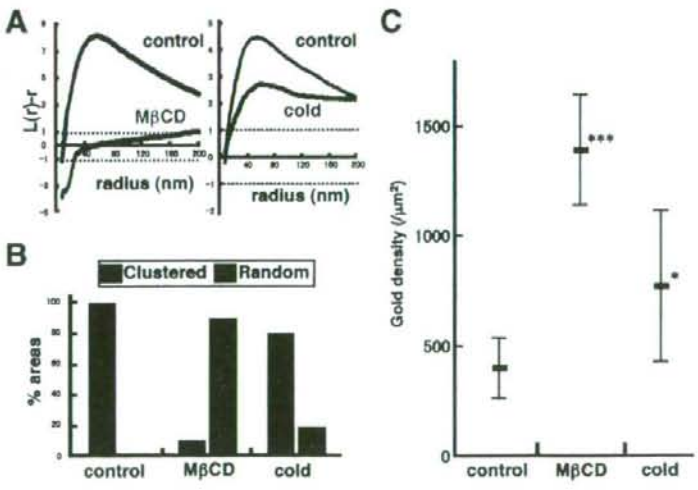

Figure 6. Changes observed after cholesterol depletion and chilling in normal mouse fibroblasts were also observed in GM1-null fibroblasts loaded with exogenous GM1. (A) The mean $L(r) - r$ curve shows a decrease of clustering after cholesterol depletion by MβCD or after chilling. The change was more drastic by cholesterol depletion than by chilling. (B and C) The proportion of areas showing random distribution as well as the average labeling density also increased significantly by cholesterol depletion or chilling.

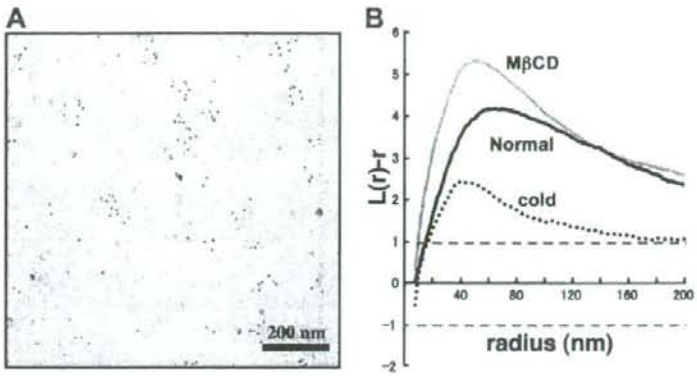

Figure 7. Distribution of PC labeled by mouse anti-PC antibody (IgM) and colloidal gold (5-nm)-conjugated goat anti-mouse Ig antibody. (A) The labeling of PC in the normal mouse fibroblast was observed as clusters in the E face, which was similar to that seen in liposomes and in other cell types (Fujimoto *et al.*, 1996). (B) The K-function analysis of 10 areas (1 × 1 μm) showed that the labeling was clustered in the normal mouse fibroblast. The clustering was observed similarly in cells depleted of cholesterol, but it decreased in chilled cells.

whereas in most areas (86.7%), the GM1 and GM3 clusters were segregated and formed independently (Figure 9, A and B). When coclustering was observed, GM1 clustering was less discrete than that observed by single labeling, which was evident in the $L(r) - r$ curve of the univariate K-function analysis (data not shown). This difference was likely caused by steric hindrance between the anti-GM1 and anti-GM3 antibodies binding to overlapping areas.

DISCUSSION

Methodological Considerations

SDS-FRL has several advantages for analyzing the distribution of membrane molecules in the submicrometer range. By freezing live cells quickly to the liquid helium temperature, the molecular motion in the cell should stop immediately. Phase separation may occur in membranes that were cooled slowly, but it was prevented by this quick-freeze method (Thompson *et al.*, 1985). In their pioneering article, Heuser and his colleagues showed that the surface of a muscle piece became frozen within 1 ms after the impact with the liquid helium-cooled copper block (Heuser *et al.*, 1979). They later found that the freezing rate is at least 10 times faster than that (Heuser, personal communication). Although details in the present experiment, the cell membrane of thin culture cells should be frozen at a better cooling rate than the muscle piece. Further sophistication in the measurement of the freezing rate is required to assess the time and spatial resolution of this method precisely.

During the freeze-fracture procedure, the specimens were kept frozen below −100°C, and the fractured membrane half was coated by evaporation of C and Pt/C to immobilize membrane molecules in situ. The physical fixation provided by the combination of quick-freezing and freeze-fracturing contrasts with chemical fixation by aldehydes in many respects. Aldehydes have only limited reactivity with membrane lipids and could even cause redistribution of membrane proteins by a cross-linking effect (Kusumi and Suzuki, 2005). More than several seconds are required for the aldehyde fixation to complete, and even after fixation, membrane molecules retain their two-dimensional mobility (Jost *et al.*, 1973; Chandler, 1984). Thus, in specimens fixed by formaldehydes, binding of probes, especially multivalent probes, could cause redistribution of membrane molecules (Mayor *et al.*, 1994). Although glutaraldehyde was shown to prevent gross redistribution of membrane proteins (Mayor *et al.*, 1994), it is unlikely to stabilize membrane lipids in the nanometer range. The membranes stabilized in replicas preclude the possibility of such artifacts caused by probes.

Compared with the conventional method that evaporates Pt/C before C, the labeling of gangliosides was improved drastically by evaporating C before Pt/C. A similar effect has been reported for some membrane proteins (Hagiwara *et*

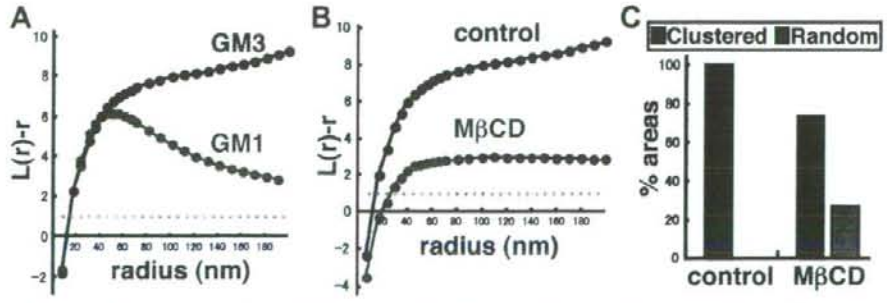

Figure 8. GM3 labeling in normal mouse fibroblasts. (A) Thirty randomly chosen areas (1 × 1 μm) were analyzed by Ripley's K-function. In contrast to GM1, the mean $L(r) - r$ curve of GM3 did not show any apparent deflection below r = 200 nm. (B) The mean $L(r) - r$ curve became lower after cholesterol depletion. (C) Classification of the 30 areas according to K-function analysis. Cholesterol depletion caused an increase in the number of areas with random distribution.

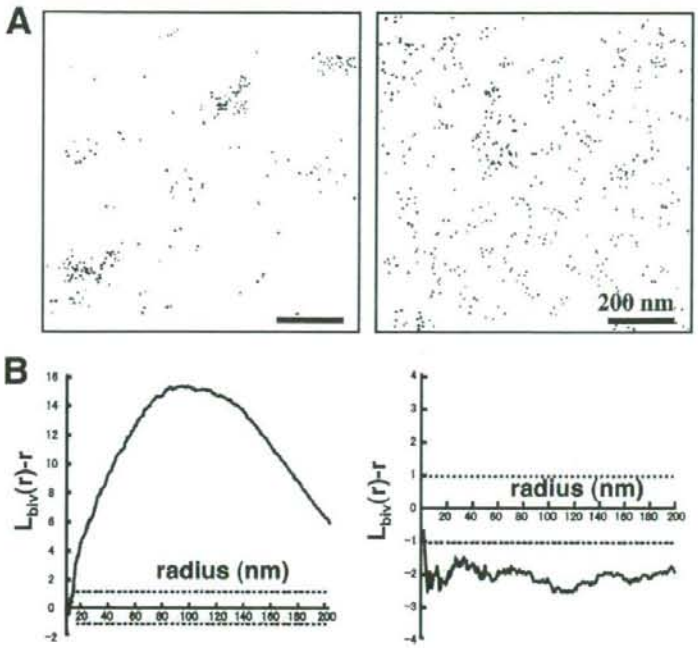

Figure 9. Double labeling of GM1 and GM3 in normal mouse fibroblasts. (A) GM1 and GM3 were marked with colloidal gold particles of different sizes, which were colored artificially: GM1, black; GM3, orange. (B) Analysis of the two areas shown in A by using a bivariate K-function. GM1 and GM3 were found to be coclustered in the left sample, but they segregated from each other in the right sample. Coclustering as shown in the left graph was seen only in 13.3% of the cases.

al., 2005). The reason for this improvement is not fully clear, but compared with Pt/C, pure C casting may allow the molecules to retain some flexibility, which may facilitate their interaction with probes. Additionally, the use of antibodies improved the GM1 labeling in SDS-FRL. CtxB worked well for immunofluorescence microscopy, but it labeled the replica to a much lesser extent than the anti-GM1 antibodies. For high-affinity binding of pentameric CtxB molecules, GM1 molecules and surrounding lipids may need to be rearranged properly, and this probably occurs frequently in the fluid membrane. The relatively low labeling by SDS-FRL may have resulted because molecules in the replica are immobilized, and they do not take an appropriate arrangement very often.

GM1 Clustering in the Cell Membrane

The GM1 labeling formed clusters with an average radius of 47.0 nm in control mouse fibroblasts. The average labeling density ranged from <100 to >1400 particles/μm^2, but clusters of similar sizes were observed irrespective of the GM1 density. In our present method, two layers of probes, either a whole IgG molecule and a F(ab')2 portion (GAR-Fab5) or a whole IgG and protein A (PAG5), were intercalated between colloidal gold (5 nm) and the antigen. Using a model experiment, the spacer distances were estimated as 16.3 ± 4.1 nm (GAR-Fab5) and 16.1 ± 5.3 nm (PAG5) (Supplemental Figure 10). This lead to a calculated size of the GM1 cluster of ~61 nm in diameter, which roughly corresponds to that which was estimated by several studies for glycosylphosphatidylinositol (GPI)-anchored protein clusters (Friedrichson and Kurzchalia, 1998; Varma and Mayor, 1998; Pralle *et al.*, 2000), but it is larger than the estimate obtained in more recent studies by using sophisticated biophysical techniques (Kusumi *et al.*, 2004; Sharma *et al.*, 2004). Ras proteins were also shown to make smaller clusters by immuno-EM of mechanically detached membranes (Plowman *et al.*, 2005). The size difference of the clusters is not surprising, however, because GPI-anchored proteins were shown to behave differently from GM1 in several instances (Schnitzer *et al.*, 1995; Simons *et al.*, 1999; Dietrich *et al.*, 2001b). It is also likely that the Ras cluster in the inner leaflet does not coincide with that of GM1 in the outer leaflet. SDS-FRL should be able to study the distribution of those proteins and to compare the cluster sizes directly.

After cholesterol depletion or incubation of cells on ice, GM1 labeling became less clustered, and areas showing random distribution increased significantly. In addition, cholesterol depletion and chilling increased the average labeling density as well as the NND. The increase of the labeling density could reflect a real increase of GM1 molecules in the plasma membrane, but the change of the aforementioned three parameters together, and above all, the virtual independence of NND values from the labeling density in control cells (Figure 4H), is more likely to suggest a dispersion of GM1 clusters by cholesterol depletion or by chilling. That is, GM1 molecules densely packed in control cells are probably not labeled efficiently due to steric hindrance, but after cholesterol depletion or chilling, they may be dispersed and more GM1 molecules may become accessible to antibodies. This possibility also suggests that the density of GM1 molecules in the cluster is underestimated in immunogold labeling.

An important question that arises from our current data is the very nature of these GM1 clusters. The clusters may be explained by the presence of rafts, or liquid-ordered (*lo*) domains, and by preferential partitioning of GM1 in the domains. The results of our chilling experiments would not seem consistent with this supposition, because low temperatures are expected to increase more ordered domains,

whereas cholesterol depletion should disrupt *lo* domains (Simons and Ikonen, 1997; Gaus *et al.*, 2003). However, as the temperature is decreased, the *lo* domain should become the dominant or percolating phase, and GM1 and other raft-philic molecules that are confined to small nonpercolating *lo* domains at the ambient temperature may adopt a dispersed distribution in the expanded *lo* domains (Meder *et al.*, 2006). Hence, the dispersed GM1 distribution after chilling can be interpreted to reflect the larger *lo* domain, or an increase of raft areas. This contrasts with the similarly dispersed GM1 distribution after cholesterol depletion, which may be caused by an increase of the liquid-disordered domains, or disruption of rafts.

However, the incomplete dissolution of the GM1 cluster and the marked regional heterogeneity upon cholesterol depletion suggest that preferential partitioning in the ordered membrane may not explain the whole phenomenon. In this context, it is notable that several studies showed formation of GM1-rich microdomains within the ordered phase of model membranes (Vie *et al.*, 1998; Yuan and Johnston, 2000; Yuan *et al.*, 2002), suggesting that glycolipids are capable of self-organization (but please note that other studies failed to observe the clustering of charged gangliosides; Thompson *et al.*, 1985; Wang and Silvius, 2003). Furthermore, the extracellular matrix, the cytoskeleton, and membrane proteins may influence distribution of membrane molecules in various ways (Edidin, 2003; Ritchie *et al.*, 2003; Mukherjee and Maxfield, 2004). These results raised a possibility that those nonraft factors are sufficient to generate the GM1 cluster in mouse fibroblasts and that rafts are not involved. Under this conjecture, the result of cholesterol depletion might be attributed to its effect on the actin cytoskeleton (Kwik *et al.*, 2003). However, we observed that manipulation of actin filaments did not affect the GM1 distribution to the extent that can explain the result of cholesterol depletion (Fujita, Cheng, and Fujimoto, unpublished observation). Moreover, chilling is not likely to affect the actin cytoskeleton in the same manner. We thus inferred that preferential partitioning in the ordered membrane is involved at least partially for the generation of GM1 clusters.

Irrespective of the mechanism that facilitates GM1 clustering in living cells, the present result has several implications. First, it has not been easy to understand why cholesterol depletion and chilling could both activate mitogen-activated protein kinase signaling (Furuchi and Anderson, 1998; Kabouridis *et al.*, 2000; Chen and Resh, 2002; Gousset *et al.*, 2002; Magee *et al.*, 2005), because the two manipulations are thought to exert opposite effects on rafts, but the present result on GM1 suggests that the two manipulations may affect the distribution of individual raft-philic molecules in the same manner and could cause a similar outcome. This tenet may be tested directly by probing fine distribution of signaling proteins that reside in the inner leaflet of the cell membrane. Second, cooling on ice has been often used to label cells for microscopy with the tacit supposition that the molecular distribution at an ambient temperature is retained. However, the present results indicated that cooling could change the distribution of some membrane molecules, so data that have been obtained from chilled cells need to be interpreted with caution.

Heterogeneous Clusters of GM1 and GM3

We observed that both GM1 and GM3 formed clusters susceptible to cholesterol depletion in normal mouse fibroblasts but that the respective clusters were segregated from each other in most cases. In migrating T cells, a distinct segregation of GM1 and GM3, i.e., GM1 in the uropod and GM3 in the leading edge, was observed (Gomez-Mouton *et al.*, 2001). Our result suggests that GM1 and GM3 also distribute differentially in other cell types, although on a much more minuscule scale. The result also implies that the high distribution density of the two gangliosides has precluded the observation of their segregation by light microscopy in the past.

Biochemical fractions enriched with GM1 and GM3 have been shown to contain different sets of signaling molecules (Iwabuchi *et al.*, 1998; Chigorno *et al.*, 2000). Those fractions are likely to correspond to the GM1 and GM3 domains that we observed, and this would raise two immediate questions. One question is whether the spatial relationship of the two domains would modulate signaling by altering molecular interactions among the signaling proteins. We observed occasional coclustering of GM1 and GM3, which suggests that the two domains could coalesce under certain conditions. It would be interesting to study how coalescence and segregation of those domains are regulated and what is brought about as a result of the domain interactions. The second question is how signaling proteins in the inner leaflet partition to one of the ganglioside domains preferentially. This may be related to the mechanism that generates separate clusters of GM1 and GM3. An intriguing possibility is that GM1 and GM3 are diversified in the ceramide portion and thus favor homologous interactions (Sonnino and Chigorno, 2000; Hakomori Si, 2002). This is not an unrealistic speculation, because glycosyltransferases for the late ganglioside biosynthetic pathways are in the distal Golgi membranes (Lannert *et al.*, 1998), which harbor cholesterol-dependent microdomains, and the probability that a GM3 molecule is processed to become GM1 may depend on the affinity of its ceramide portion to the microdomain where the enzymes exist. As a result, gangliosides remaining as GM3, and those that became GM1, are likely to make homologous clusters more often than heterogeneous gangliosides. Analysis of the ceramide composition of gangliosides is awaited to test the possibility.

Although the underlying mechanism needs to be explored further, our result showed that GM1 and GM3 exist as distinct clusters in the native cell membrane. But the GM1 and GM3 clusters may not be the only microdomains that are affected by cholesterol depletion, and additional microdomains with variable contents are likely to coexist (Marwali *et al.*, 2003; Nagatsuka *et al.*, 2003; Brugger *et al.*, 2004; Kiyokawa *et al.*, 2005). How all those heterogeneous microdomains are formed and how their mutual relationship is controlled warrant further investigation. Hopefully, the present method would help to address these unsolved questions in the near future.

ACKNOWLEDGMENTS

We thank Drs. Atsuyuki Okabe and Ken-ichiro Shimatani for advice on point pattern analysis, Dr. John Hancock for providing the K-function program, Dr. Masato Umeda for anti-PC antibody, Drs. Akihiro Kusumi and John E. Heuser for helpful discussions, and Kumi Tauchi-Sato and Tetsuo Okumura for assistance. This work was supported by grants-in-aid for scientific research and the 21st Century Center of Excellence Program "Integrated Molecular Medicine for Neuronal and Neoplastic Disorders" of the Ministry of Education, Culture, Sports, Science and Technology of the Japanese Government.

REFERENCES

Brugger, B., Graham, C., Leibrecht, I., Mombelli, E., Jen, A., Wieland, F., and Morris, R. (2004). The membrane domains occupied by glycosylphosphatidylinositol-anchored prion protein and Thy-1 differ in lipid composition. J. Biol. Chem. 279, 7530–7536.

Chandler, D. E. (1984). Comparison of quick-frozen and chemically fixed sea-urchin eggs: structural evidence that cortical granule exocytosis is preceded by a local increase in membrane mobility. J. Cell Sci. *72*, 23–36.

Chen, X., and Resh, M. D. (2002). Cholesterol depletion from the plasma membrane triggers ligand-independent activation of the epidermal growth factor receptor. J. Biol. Chem. *277*, 49631–49637.

Chigorno, V., Palestini, P., Sciannamblo, M., Dolo, V., Pavan, A., Tettamanti, G., and Sonnino, S. (2000). Evidence that ganglioside enriched domains are distinct from caveolae in MDCK II and human fibroblast cells in culture. Eur. J. Biochem. *267*, 4187–4197.

Dietrich, C., Bagatolli, L. A., Volovyk, Z. N., Thompson, N. L., Levi, M., Jacobson, K., and Gratton, E. (2001a). Lipid rafts reconstituted in model membranes. Biophys. J. *80*, 1417–1428.

Dietrich, C., Volovyk, Z. N., Levi, M., Thompson, N. L., and Jacobson, K. (2001b). Partitioning of Thy-1, GM1, and cross-linked phospholipid analogs into lipid rafts reconstituted in supported model membrane monolayers. Proc. Natl. Acad. Sci. USA *98*, 10642–10647.

Edidin, M. (2003). The state of lipid rafts: from model membranes to cells. Annu. Rev. Biophys. Biomol. Struct. *32*, 257–283.

Friedrichson, T., and Kurzchalia, T. V. (1998). Microdomains of GPI-anchored proteins in living cells revealed by crosslinking. Nature *394*, 802–805.

Fujimoto, K. (1995). Freeze-fracture replica electron microscopy combined with SDS digestion for cytochemical labeling of integral membrane proteins. Application to the immunogold labeling of intercellular junctional complexes. J. Cell Sci. *108*, 3443–3449.

Fujimoto, K., Umeda, M., and Fujimoto, T. (1996). Transmembrane phospholipid distribution revealed by freeze-fracture replica labeling. J. Cell Sci. *109*, 2453–2460.

Fujimoto, T. (1996). GPI-anchored proteins, glycosphingolipids, and sphingomyelin are sequestered to caveolae only after crosslinking. J. Histochem. Cytochem. *44*, 929–941.

Fujimoto, T., and Fujimoto, K. (1997). Metal sandwich method to quick-freeze monolayer cultured cells for freeze-fracture. J. Histochem. Cytochem. *45*, 595–598.

Furuchi, T., and Anderson, R. G. (1998). Cholesterol depletion of caveolae causes hyperactivation of extracellular signal-related kinase (ERK). J. Biol. Chem. *273*, 21099–21104.

Gaus, K., Gratton, E., Kable, E. P., Jones, A. S., Gelissen, I., Kritharides, L., and Jessup, W. (2003). Visualizing lipid structure and raft domains in living cells with two-photon microscopy. Proc. Natl. Acad. Sci. USA *100*, 15554–15559.

Gomez-Mouton, C., Abad, J. L., Mira, E., Lacalle, R. A., Gallardo, E., Jimenez-Baranda, S., Illa, I., Bernad, A., Manes, S., and Martinez, A. C. (2001). Segregation of leading-edge and uropod components into specific lipid rafts during T cell polarization. Proc. Natl. Acad. Sci. USA *98*, 9642–9647.

Gousset, K., Wolkers, W. F., Tsvetkova, N. M., Oliver, A. E., Field, C. L., Walker, N. J., Crowe, J. H., and Tablin, F. (2002). Evidence for a physiological role for membrane rafts in human platelets. J. Cell. Physiol. *190*, 117–128.

Hagiwara, A., Fukazawa, Y., Deguchi-Tawarada, M., Ohtsuka, T., and Shigemoto, R. (2005). Differential distribution of release-related proteins in the hippocampal CA3 area as revealed by freeze-fracture replica labeling. J. Comp. Neurol. *489*, 195–216.

Hakomori Si, S. I. (2002). Inaugural article: the glycosynapse. Proc. Natl. Acad. Sci. USA *99*, 225–232.

Heerklotz, H. (2002). Triton promotes domain formation in lipid raft mixtures. Biophys. J. *83*, 2693–2701.

Heider, J. G., and Boyett, R. L. (1978). The picomole determination of free and total cholesterol in cells in culture. J. Lipid Res. *19*, 514–518.

Heuser, J. E., Reese, T. S., Dennis, M. J., Jan, Y., Jan, L., and Evans, L. (1979). Synaptic vesicle exocytosis captured by quick freezing and correlated with quantal transmitter release. J. Cell Biol. *81*, 275–300.

Iwabuchi, K., Handa, K., and Hakomori, S. (1998). Separation of "glycosphingolipid signaling domain" from caveolin-containing membrane fraction in mouse melanoma B16 cells and its role in cell adhesion coupled with signaling. J. Biol. Chem. *273*, 33766–33773.

Jost, P., Brooks, U. J., and Griffith, O. H. (1973). Fluidity of phospholipid bilayers and membranes after exposure to osmium tetroxide and gluteraldehyde. J. Mol. Biol. *76*, 313–318.

Kabouridis, P. S., Janzen, J., Magee, A. L., and Ley, S. C. (2000). Cholesterol depletion disrupts lipid rafts and modulates the activity of multiple signaling pathways in T lymphocytes. Eur. J. Immunol. *30*, 954–963.

Kenworthy, A. K., Nichols, B. J., Remmert, C. L., Hendrix, G. M., Kumar, M., Zimmerberg, J., and Lippincott-Schwartz, J. (2004). Dynamics of putative raft-associated proteins at the cell surface. J. Cell Biol. *165*, 735–746.

Kenworthy, A. K., Petranova, N., and Edidin, M. (2000). High-resolution FRET microscopy of cholera toxin B-subunit and GPI-anchored proteins in cell plasma membranes. Mol. Biol. Cell *11*, 1645–1655.

Kiyokawa, E., Baba, T., Otsuka, N., Makino, A., Ohno, S., and Kobayashi, T. (2005). Spatial and functional heterogeneity of sphingolipid-rich membrane domains. J. Biol. Chem. *280*, 24072–24084.

Korlach, J., Schwille, P., Webb, W. W., and Feigenson, G. W. (1999). Characterization of lipid bilayer phases by confocal microscopy and fluorescence correlation spectroscopy. Proc. Natl. Acad. Sci. USA *96*, 8461–8466.

Kusumi, A., Koyama-Honda, I., and Suzuki, K. (2004). Molecular dynamics and interactions for creation of stimulation-induced stabilized rafts from small unstable steady-state rafts. Traffic *5*, 213–230.

Kusumi, A., and Suzuki, K. (2005). Toward understanding the dynamics of membrane-raft-based molecular interactions. Biochim. Biophys. Acta *1746*, 234–251.

Kusunoki, S., Shimizu, J., Chiba, A., Ugawa, Y., Hitoshi, S., and Kanazawa, I. (1996). Experimental sensory neuropathy induced by sensitization with ganglioside GD1b. Ann. Neurol. *39*, 424–431.

Kwik, J., Boyle, S., Fooksman, D., Margolis, L., Sheetz, M. P., and Edidin, M. (2003). Membrane cholesterol, lateral mobility, and the phosphatidylinositol 4,5-bisphosphate-dependent organization of cell actin. Proc. Natl. Acad. Sci. USA *100*, 13964–13969.

Lannert, H., Gorgas, K., Meissner, I., Wieland, F. T., and Jeckel, D. (1998). Functional organization of the Golgi apparatus in glycosphingolipid biosynthesis. Lactosylceramide and subsequent glycosphingolipids are formed in the lumen of the late Golgi. J. Biol. Chem. *273*, 2939–2946.

Magee, A. I., Adler, J., and Parmryd, I. (2005). Cold-induced coalescence of T-cell plasma membrane microdomains activates signalling pathways. J. Cell Sci. *118*, 3141–3151.

Marwali, M. R., Rey-Ladino, J., Dreolini, L., Shaw, D., and Takei, F. (2003). Membrane cholesterol regulates LFA-1 function and lipid raft heterogeneity. Blood *102*, 215–222.

Mayor, S., and Rao, M. (2004). Rafts: scale-dependent, active lipid organization at the cell surface. Traffic *5*, 231–240.

Mayor, S., Rothberg, K. G., and Maxfield, F. R. (1994). Sequestration of GPI-anchored proteins in caveolae triggered by cross-linking. Science *264*, 1948–1951.

Meder, D., Moreno, M. J., Verkade, P., Vaz, W. L., and Simons, K. (2006). Phase coexistence and connectivity in the apical membrane of polarized epithelial cells. Proc. Natl. Acad. Sci. USA *103*, 329–334.

Mukherjee, S., and Maxfield, F. R. (2004). Membrane domains. Annu. Rev. Cell Dev. Biol. *20*, 839–866.

Munro, S. (2003). Lipid rafts: elusive or illusive? Cell *115*, 377–388.

Nagatsuka, Y. *et al.* (2003). Carbohydrate-dependent signaling from the phosphatidylglucoside-based microdomain induces granulocytic differentiation of HL60 cells. Proc. Natl. Acad. Sci. USA *100*, 7454–7459.

Nam, K. S., Igarashi, K., Umeda, M., and Inoue, K. (1990). Production and characterization of monoclonal antibodies that specifically bind to phosphatidylcholine. Biochim. Biophys. Acta *1046*, 89–96.

Nichols, B. J. (2003). GM1-containing lipid rafts are depleted within clathrin-coated pits. Curr. Biol. *13*, 686–690.

Parton, R. G. (1994). Ultrastructural localization of gangliosides; GM1 is concentrated in caveolae. J. Histochem. Cytochem. *42*, 155–166.

Plowman, S. J., Muncke, C., Parton, R. G., and Hancock, J. F. (2005). H-ras, K-ras, and inner plasma membrane raft proteins operate in nanoclusters with differential dependence on the actin cytoskeleton. Proc. Natl. Acad. Sci. USA *102*, 15500–15505.

Pralle, A., Keller, P., Florin, E. L., Simons, K., and Horber, J. K. (2000). Sphingolipid-cholesterol rafts diffuse as small entities in the plasma membrane of mammalian cells. J. Cell Biol. *148*, 997–1008.

Prior, I. A., Muncke, C., Parton, R. G., and Hancock, J. F. (2003). Direct visualization of Ras proteins in spatially distinct cell surface microdomains. J. Cell Biol. *160*, 165–170.

Ripley, B. D. (1977). Modeling spatial patterns. J. R. Stat. Soc. Ser. B *39*, 172–212.

Ripley, B. D. (1979). Tests of randomness for spatial point patterns. J. R. Stat. Soc. Ser. B *41*, 368–374.

Ritchie, K., Iino, R., Fujiwara, T., Murase, K., and Kusumi, A. (2003). The fence and picket structure of the plasma membrane of live cells as revealed by single molecule techniques. Mol. Membr. Biol. *20*, 13–18.

Schnitzer, J. E., McIntosh, D. P., Dvorak, A. M., Liu, J., and Oh, P. (1995). Separation of caveolae from associated microdomains of GPI-anchored proteins. Science *269*, 1435–1439.

Schwarzmann, G., Hoffmann-Bleihauer, P., Schubert, J., Sandhoff, K., and Marsh, D. (1983). Incorporation of ganglioside analogues into fibroblast cell membranes. A spin-label study. Biochemistry *22*, 5041–5048.

Sharma, P., Varma, R., Sarasij, R. C., Ira, Gousset, K., Krishnamoorthy, G., Rao, M., and Mayor, S. (2004). Nanoscale organization of multiple GPI-anchored proteins in living cell membranes. Cell *116*, 577–589.

Simons, K., and Ikonen, E. (1997). Functional rafts in cell membranes. Nature *387*, 569–572.

Simons, M., Friedrichson, T., Schulz, J. B., Pitto, M., Masserini, M., and Kurzchalia, T. V. (1999). Exogenous administration of gangliosides displaces GPI-anchored proteins from lipid microdomains in living cells. Mol. Biol. Cell *10*, 3187–3196.

Sonnino, S., and Chigorno, V. (2000). Ganglioside molecular species containing C18- and C20-sphingosine in mammalian nervous tissues and neuronal cell cultures. Biochim. Biophys. Acta *1469*, 63–77.

Takamiya, K. *et al.* (1996). Mice with disrupted GM2/GD2 synthase gene lack complex gangliosides but exhibit only subtle defects in their nervous system. Proc. Natl. Acad. Sci. USA *93*, 10662–10667.

Taki, T., and Ishikawa, D. (1997). TLC blotting: application to microscale analysis of lipids and as a new approach to lipid-protein interaction. Anal. Biochem. *251*, 135–143.

Thompson, T. E., Allietta, M., Brown, R. E., Johnson, M. L., and Tillack, T. W. (1985). Organization of ganglioside GM1 in phosphatidylcholine bilayers. Biochim. Biophys. Acta *817*, 229–237.

Varma, R., and Mayor, S. (1998). GPI-anchored proteins are organized in submicron domains at the cell surface. Nature *394*, 798–801.

Vie, V., Van Mau, N., Lesniewska, E., Goudonnet, J. P., Heitz, F., and Le Grimelle, C. (1998). Distribution of ganglioside GM1 between two-component, two-phase phosphatidylcholine monolayers. Langmuir *14*, 4754–4783.

Wang, T. Y., and Silvius, J. R. (2003). Sphingolipid partitioning into ordered domains in cholesterol-free and cholesterol-containing lipid bilayers. Biophys. J. *84*, 367–378.

Williams, M. A., and McCluer, R. H. (1980). The use of Sep-Pak C18 cartridges during the isolation of gangliosides. J. Neurochem. *35*, 266–269.

Yuan, C., Furlong, J., Burgos, P., and Johnston, L. J. (2002). The size of lipid rafts: an atomic force microscopy study of ganglioside GM1 domains in sphingomyelin/DOPC/cholesterol membranes. Biophys. J. *82*, 2526–2535.

Yuan, C., and Johnston, L. J. (2000). Distribution of ganglioside GM1 in L-alpha-dipalmitoylphosphatidylcholine/cholesterol monolayers: a model for lipid rafts. Biophys. J. *79*, 2768–2781.

Zhou, X., and Arthur, G. (1992). Improved procedures for the determination of lipid phosphorus by malachite green. J. Lipid Res. *33*, 1233–1236.